



Grasping

38. Grasping

Domenico Prattichizzo, Jeffrey C. Trinkle

This chapter introduces fundamental models of grasp analysis. The overall model is a coupling of models that define contact behavior with widely used models of rigid-body kinematics and dynamics. The contact model essentially boils down to the selection of components of contact force and moment that are transmitted through each contact. Mathematical properties of the complete model naturally give rise to five primary grasp types whose physical interpretations provide insight for grasp and manipulation planning.

After introducing the basic models and types of grasps, this chapter focuses on the most important grasp characteristic: complete restraint. A grasp with complete restraint prevents loss of contact and thus is very secure. Two primary restraint properties are *form closure* and *force closure*. A form closure grasp guarantees maintenance of contact as long as the links of the hand and the object are well-approximated as rigid and as long as the joint actuators are sufficiently strong. As will be seen, the primary difference between form closure and force closure grasps is the latter's reliance on contact friction. This translates into requiring fewer contacts to achieve force closure than form closure.

The goal of this chapter is to give a thorough understanding of the all-important grasp properties of form and force closure. This will be done through detailed derivations of grasp models and

38.1 Models and Definitions	956
38.1.1 Velocity Kinematics	957
38.1.2 Dynamics and Equilibrium	960
38.2 Controllable Twists and Wrenches	961
38.2.1 Grasp Classifications	962
38.2.2 Limitations of Rigid-Body Formulation	963
38.2.3 Desirable Properties	963
38.3 Compliant Grasps	965
38.4 Restraint Analysis	967
38.4.1 Form Closure	968
38.4.2 Force Closure	972
38.5 Examples	975
38.5.1 Example 1: Grasped Sphere	975
38.5.2 Example 2: Grasped Polygon in the Plane	978
38.5.3 Example 3: Hyperstatic Grasps	980
38.5.4 Example 4: Duality	983
38.5.5 Example 5: Form Closure	983
38.6 Conclusion and Further Reading	985
Video-References	986
References	986

discussions of illustrative examples. For an in-depth historical perspective and a treasure-trove bibliography of papers addressing a wide range of topics in grasping, the reader is referred to [38.1].

Mechanical hands were developed to give robots the ability to grasp objects of varying geometric and physical properties. The first robotic hand designed for dexterous manipulation was the Salisbury Hand (Fig. 38.1) [38.2]. It has three three-jointed fingers;

enough to control all six degrees of freedom of an object and the grip pressure. The fundamental grasp modeling and analysis done by Salisbury provides a basis for grasp synthesis and dexterous manipulation research which continues today. Some of the most ma-

ture analysis techniques are embedded in the widely used software *GraspIt!* [38.3] and *SynGrasp* [38.4, 5]. *GraspIt!* contains models for several robot hands and provides tools for grasp selection, dynamic grasp simulation, and visualization. *SynGrasp* is a MATLAB Toolbox that can be obtained from [38.6] and provides models and functions for grasp analysis with both fully and underactuated hands. It can be a useful educational tool to get acquainted with the mathemat-

ical framework of robotic grasping described in this Chapter. Over the years since the Salisbury Hand was built, many articulated robot hands have been developed. Nearly all of these have one actuator per joint or fewer. A notable exception is the *DLR hand arm system* developed by DLR (Deutsches Zentrum für Luft- und Raumfahrt), which has two actuators per joint that drive each joint independently with two antagonistic tendons (Fig. 38.7) [38.7].

38.1 Models and Definitions

A mathematical model of grasping must be capable of predicting the behavior of the hand and object under various loading conditions that may arise during grasping. Generally, the most desirable behavior is grasp maintenance in the face of unknown disturbing forces and moments applied to the object. Typically these disturbances arise from inertia forces which become appreciable during high-speed manipulation or applied forces such as those due to gravity. Grasp maintenance means that the contact forces applied by the hand are such that they prevent contact separation and unwanted contact sliding. The special class of grasps that can be maintained for every possible disturbing load is known as closure grasps. Figure 38.1 shows the Salisbury Hand [38.2, 8], executing a closure grasp of an object by wrapping its fingers around it and pressing it against its palm. Formal definitions, analysis, and computational tests for closure will be presented in Sect. 38.4.

Figure 38.2 illustrates some of the main quantities that will be used to model grasping systems. Assume that the links of the hand and the object are rigid and that there is a unique, well-defined tangent plane at each contact point. Let $\{N\}$ represent a conveniently chosen inertial frame fixed in the workspace. The frame $\{B\}$

is fixed to the object with its origin defined relative to $\{N\}$ by the vector $\mathbf{p} \in \mathbb{R}^3$, where \mathbb{R}^3 denotes three-dimensional Euclidean space. A convenient choice for \mathbf{p} is the center of mass of the object. The position of contact point i in $\{N\}$ is defined by the vector $\mathbf{c}_i \in \mathbb{R}^3$. At contact point i , we define a frame $\{C\}_i$, with axes $\{\hat{\mathbf{n}}_i, \hat{\mathbf{t}}_i, \hat{\mathbf{o}}_i\}$ ($\{C\}_1$ is shown in *exploded view*). The unit vector $\hat{\mathbf{n}}_i$ is normal to the contact tangent plane and directed toward the object. The other two unit vectors are orthogonal and lie in the tangent plane of the contact.

Let the joints be numbered from 1 to n_q . Denote by $\mathbf{q} = [q_1 \cdots q_{n_q}]^T \in \mathbb{R}^{n_q}$ the vector of joint displacements, where the superscript T indicates matrix transposition. Also, let $\boldsymbol{\tau} = [\tau_1 \cdots \tau_{n_q}]^T \in \mathbb{R}^{n_q}$ represent joint loads (forces in prismatic joints and torques in revolute joints). These loads can result from actuator actions, other applied forces, and inertia forces. They could also arise from interaction at the contacts between the object and hand. However, it will be convenient to sep-



Fig. 38.1 The Salisbury Hand grasping an object

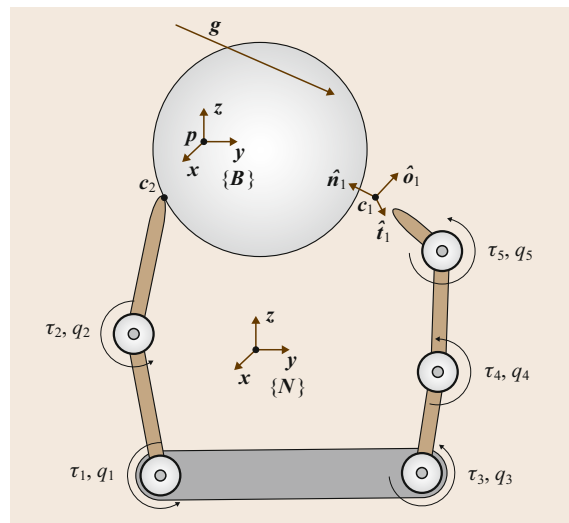


Fig. 38.2 Main quantities for grasp analysis

arate joint loads into two components: those arising from contacts and those arising from all other sources. Throughout this Chapter, non-contact loads will be denoted by τ .

Let $\mathbf{u} \in \mathbb{R}^{n_u}$ denote the vector describing the position and orientation of $\{\mathcal{B}\}$ relative to $\{\mathcal{N}\}$. For planar systems $n_u = 3$. For spatial systems, n_u is three plus the number of parameters used to represent orientation; typically three (for Euler angles) or four (for unit quaternions). Denote by $\mathbf{v} = [\mathbf{v}^T \boldsymbol{\omega}^T]^T \in \mathbb{R}^{n_v}$, the twist of the object described in $\{\mathcal{N}\}$. It is composed of the translational velocity $\mathbf{v} \in \mathbb{R}^3$ of the point \mathbf{p} and the angular velocity $\boldsymbol{\omega} \in \mathbb{R}^3$ of the object, both expressed in $\{\mathcal{N}\}$. A twist of a rigid body can be referred to any convenient frame fixed to the body. The components of the referred twist represent the velocity of the origin of the new frame and the angular velocity of the body, both expressed in the new frame (Table 38.1). For a rigorous treatment of twists and wrenches see [38.9, 10]. Note that for planar systems, $\mathbf{v} \in \mathbb{R}^2$, $\boldsymbol{\omega} \in \mathbb{R}$, and so $n_v = 3$.

Another important point is $\dot{\mathbf{u}} \neq \mathbf{v}$. Instead, these variables are related by the matrix \mathbf{V} as

$$\dot{\mathbf{u}} = \mathbf{V}\mathbf{v}, \quad (38.1)$$

where the matrix $\mathbf{V} \in \mathbb{R}^{n_u \times n_v}$ is not generally square, but nonetheless satisfies $\mathbf{V}^T \mathbf{V} = \mathbf{I}$ [38.11], where \mathbf{I} is the identity matrix, and the dot over the \mathbf{u} implies differentiation with respect to time. Note that for planar systems, $\mathbf{V} = \mathbf{I} \in \mathbb{R}^{3 \times 3}$.

Let $\mathbf{f} \in \mathbb{R}^3$ be the force applied to the object at the point \mathbf{p} and let $\mathbf{m} \in \mathbb{R}^3$ be the applied moment. These are combined into the object load, or wrench, vector denoted by $\mathbf{g} = [\mathbf{f}^T \mathbf{m}^T]^T \in \mathbb{R}^{n_v}$, where \mathbf{f} and \mathbf{m} are expressed in $\{\mathcal{N}\}$. Like twists, wrenches can be referred to any convenient frame fixed to the body. One can think of this as translating the line of application of the force until it contains the origin of the new frame, then adjusting the moment component of the wrench to offset the moment induced by moving the line of the force. Last, the force and adjusted moment are expressed in the new frame. As done with the joint loads, the object wrench will be partitioned into two main parts: contact and non-contact wrenches. Throughout this chapter, \mathbf{g} will denote the non-contact wrench on the object.

38.1.1 Velocity Kinematics

The material in this chapter is valid for a wide range of robot hands and other grasping mechanisms. The hand is assumed to be composed of a palm that serves as the common base for any number of fingers, each with any number of joints. The formulations given in this chapter are expressed explicitly in terms of only

Table 38.1 Primary notation for grasp analysis

Notation	Definition
n_c	Number of contacts
n_q	Number of joints of the hand
n_v	Number of degrees of freedom of object
n_λ	Number of contact wrench components
$\mathbf{q} \in \mathbb{R}^{n_q}$	Joint displacements
$\dot{\mathbf{q}} \in \mathbb{R}^{n_q}$	Joint velocities
$\boldsymbol{\tau} \in \mathbb{R}^{n_q}$	Non-contact joint loads
$\mathbf{u} \in \mathbb{R}^{n_u}$	Position and orientation of object
$\mathbf{v} \in \mathbb{R}^{n_v}$	Twist of object
$\mathbf{g} \in \mathbb{R}^{n_v}$	Non-contact object wrench
$\boldsymbol{\lambda} \in \mathbb{R}^{n_\lambda}$	Transmitted contact wrenches
$\mathbf{v}_{cc} \in \mathbb{R}^{n_\lambda}$	Transmitted contact twists
$\{\mathcal{B}\}$	Frame fixed in object
$\{\mathcal{C}\}_i$	Frame at contact i
$\{\mathcal{N}\}$	Inertial frame

revolute and prismatic joints. However, most other common joints can be modeled by combinations of revolute and prismatic joints (e.g., cylindrical and planar). Any number of contacts may occur between any link and the object.

Grasp Matrix and Hand Jacobian

Two matrices are of the utmost importance in grasp analysis: the *grasp matrix* \mathbf{G} and the *hand Jacobian* \mathbf{J} . These matrices define the relevant velocity kinematics and force transmission properties of the contacts. The following derivations of \mathbf{G} and \mathbf{J} will be done under the assumption that the system is three-dimensional ($n_v = 6$). Changes for planar systems will be noted later.

Each contact should be considered as two coincident points; one on the hand and one on the object. The hand Jacobian maps the joint velocities to the twists of the hand to the contact frames, while the transpose of the grasp matrix maps the object twist to the contact frames. Finger joint motions induce a rigid body motion in each link of the hand. It is implicit in the terminology, twists of the hand, that the twist referred to contact i is the twist of the link involved in contact i . Thus these matrices can be derived from the transforms that change the reference frame of a twist.

To derive the grasp matrix, let $\boldsymbol{\omega}_{\text{obj}}^{\mathcal{N}}$ denote the angular velocity of the object expressed in $\{\mathcal{N}\}$ and let $\mathbf{v}_{i,\text{obj}}^{\mathcal{N}}$, also expressed in $\{\mathcal{N}\}$, denote the velocity of the point on the object coincident with the origin of $\{\mathcal{C}\}_i$. These velocities can be obtained from the object twist referred to $\{\mathcal{N}\}$ as

$$\begin{pmatrix} \mathbf{v}_{i,\text{obj}}^{\mathcal{N}} \\ \boldsymbol{\omega}_{\text{obj}}^{\mathcal{N}} \end{pmatrix} = \mathbf{P}_i^T \mathbf{v}, \quad (38.2)$$

where

$$\mathbf{P}_i = \begin{pmatrix} \mathbf{I}_{3 \times 3} & \mathbf{0} \\ \mathbf{S}(\mathbf{c}_i - \mathbf{p}) & \mathbf{I}_{3 \times 3} \end{pmatrix} \quad (38.3)$$

$\mathbf{I}_{3 \times 3} \in \mathbb{R}^{3 \times 3}$ is the identity matrix, and $\mathbf{S}(\mathbf{c}_i - \mathbf{p})$ is the cross product matrix, that is, given a three-vector $\mathbf{r} = [r_x \ r_y \ r_z]^T$, $\mathbf{S}(\mathbf{r})$ is defined as follows

$$\mathbf{S}(\mathbf{r}) = \begin{pmatrix} 0 & -r_z & r_y \\ r_z & 0 & -r_x \\ -r_y & r_x & 0 \end{pmatrix}.$$

The object twist referred to $\{\mathbf{C}\}_i$ is simply the vector on the left-hand side of (38.2) expressed in $\{\mathbf{C}\}_i$.

Let $\mathbf{R}_i = (\hat{\mathbf{n}}_i \hat{\mathbf{t}}_i \hat{\mathbf{o}}_i) \in \mathbb{R}^{3 \times 3}$ represent the orientation of the i -th contact frame $\{\mathbf{C}\}_i$ with respect to the inertial frame (the unit vectors $\hat{\mathbf{n}}_i$, $\hat{\mathbf{t}}_i$, and $\hat{\mathbf{o}}_i$ are expressed in $\{\mathcal{N}\}$). Then the object twist referred to $\{\mathbf{C}\}_i$ is given as

$$\mathbf{v}_{i,\text{obj}} = \bar{\mathbf{R}}_i^T \begin{pmatrix} \mathbf{v}_{i,\text{obj}}^N \\ \boldsymbol{\omega}_{\text{obj}}^N \end{pmatrix}, \quad (38.4)$$

where $\bar{\mathbf{R}}_i = \text{Blockdiag}(\mathbf{R}_i, \mathbf{R}_i) = \begin{pmatrix} \mathbf{R}_i & \mathbf{0} \\ \mathbf{0} & \mathbf{R}_i \end{pmatrix} \in \mathbb{R}^{6 \times 6}$.

Substituting $\mathbf{P}_i^T \mathbf{v}$ from (38.2) into (38.4) yields the partial grasp matrix $\tilde{\mathbf{G}}_i^T \in \mathbb{R}^{6 \times 6}$, that maps the object twist from $\{\mathcal{N}\}$ to $\{\mathbf{C}\}_i$

$$\mathbf{v}_{i,\text{obj}} = \tilde{\mathbf{G}}_i^T \mathbf{v}, \quad (38.5)$$

where

$$\tilde{\mathbf{G}}_i^T = \bar{\mathbf{R}}_i^T \mathbf{P}_i^T. \quad (38.6)$$

The hand Jacobian can be derived similarly. Let $\boldsymbol{\omega}_{i,\text{hnd}}^N$ be the angular velocity of the link of the hand touching the object at contact i , expressed in $\{\mathcal{N}\}$, and define $\mathbf{v}_{i,\text{hnd}}^N$ as the translational velocity of contact i on the hand, expressed in $\{\mathcal{N}\}$. These velocities are related to the joint velocities through the matrix \mathbf{Z}_i whose columns are the Plücker coordinates of the axes of the joints [38.9, 10]. We have

$$\begin{pmatrix} \mathbf{v}_{i,\text{hnd}}^N \\ \boldsymbol{\omega}_{i,\text{hnd}}^N \end{pmatrix} = \mathbf{Z}_i \dot{\mathbf{q}}, \quad (38.7)$$

where $\mathbf{Z}_i \in \mathbb{R}^{6 \times n_q}$ is defined as

$$\mathbf{Z}_i = \begin{pmatrix} \mathbf{d}_{i,1} & \cdots & \mathbf{d}_{i,n_q} \\ \boldsymbol{\kappa}_{i,1} & \cdots & \boldsymbol{\kappa}_{i,n_q} \end{pmatrix}, \quad (38.8)$$

with the vectors $\mathbf{d}_{i,j}, \boldsymbol{\kappa}_{i,j} \in \mathbb{R}^3$ defined as

$$\mathbf{d}_{i,j} = \begin{cases} \mathbf{0}_{3 \times 1} & \text{if contact force } i \text{ does} \\ & \text{not affect joint } j, \\ \hat{\mathbf{z}}_j & \text{if joint } j \text{ is prismatic,} \\ \mathbf{S}(\mathbf{c}_i - \boldsymbol{\xi}_j)^T \hat{\mathbf{z}}_j & \text{if joint } j \text{ is revolute,} \end{cases}$$

$$\boldsymbol{\kappa}_{i,j} = \begin{cases} \mathbf{0}_{3 \times 1} & \text{if contact force } i \text{ does} \\ & \text{not affect joint } j, \\ \mathbf{0}_{3 \times 1} & \text{if joint } j \text{ is prismatic,} \\ \hat{\mathbf{z}}_j & \text{if joint } j \text{ is revolute,} \end{cases}$$

where $\boldsymbol{\xi}_j$ is the origin of the coordinate frame associated with the j -th joint and $\hat{\mathbf{z}}_j$ is the unit vector in the direction of the z -axis in the same frame, as shown in Fig. 38.12. Both vectors are expressed in $\{\mathcal{N}\}$. These frames may be assigned by any convenient method, for example, the Denavit–Hartenberg method [38.12]. The $\hat{\mathbf{z}}_j$ -axis is the rotational axis for revolute joints and the direction of translation for prismatic joints.

The final step in referring the hand twists to the contact frames is change the frame of expression of $\mathbf{v}_{i,\text{hnd}}^N$ and $\boldsymbol{\omega}_{i,\text{hnd}}^N$ to $\{\mathbf{C}\}_i$

$$\mathbf{v}_{i,\text{hnd}} = \bar{\mathbf{R}}_i^T \begin{pmatrix} \mathbf{v}_{i,\text{hnd}}^N \\ \boldsymbol{\omega}_{i,\text{hnd}}^N \end{pmatrix}. \quad (38.9)$$

Combining (38.9) and (38.7) yields the partial hand Jacobian $\tilde{\mathbf{J}}_i \in \mathbb{R}^{6 \times n_q}$, which relates the joint velocities to the contact twists on the hand

$$\mathbf{v}_{i,\text{hnd}} = \tilde{\mathbf{J}}_i \dot{\mathbf{q}}, \quad (38.10)$$

where

$$\tilde{\mathbf{J}}_i = \bar{\mathbf{R}}_i^T \mathbf{Z}_i. \quad (38.11)$$

To simplify notation, stack all the twists on the hand and object into the vectors $\mathbf{v}_{c,\text{hnd}} \in \mathbb{R}^{6n_c}$ and $\mathbf{v}_{c,\text{obj}} \in \mathbb{R}^{6n_c}$ as follows

$$\mathbf{v}_{c,\xi} = \left(\mathbf{v}_{1,\xi}^T \quad \cdots \quad \mathbf{v}_{n_c,\xi}^T \right)^T, \quad \xi = \{\text{obj}, \text{hnd}\}.$$

Now the complete grasp matrix $\tilde{\mathbf{G}} \in \mathbb{R}^{6 \times 6n_c}$ and complete hand Jacobian $\tilde{\mathbf{J}} \in \mathbb{R}^{6n_c \times n_q}$ relate the various velocity quantities as follows

$$\mathbf{v}_{c,\text{obj}} = \tilde{\mathbf{G}}^T \mathbf{v}, \quad (38.12)$$

$$\mathbf{v}_{c,\text{hnd}} = \tilde{\mathbf{J}} \dot{\mathbf{q}}, \quad (38.13)$$

where

$$\tilde{\mathbf{G}}^T = \begin{pmatrix} \tilde{\mathbf{G}}_1^T \\ \vdots \\ \tilde{\mathbf{G}}_{n_c}^T \end{pmatrix}, \quad \tilde{\mathbf{J}} = \begin{pmatrix} \tilde{\mathbf{J}}_1 \\ \vdots \\ \tilde{\mathbf{J}}_{n_c} \end{pmatrix}. \quad (38.14)$$

The term *complete* is used to emphasize that all $6n_c$ twist components at the contacts are included in the mapping. See Example 1, Part 1 and Example 3, Part 1 at the end of this chapter for clarification.

Contact Modeling

Contacts play a central role in grasping. Contacts allow to impose a given motion to the object or to apply a given force through the object. All grasping actions go through contacts whose model and control is crucial in grasping. Three contact models useful for grasp analysis are reviewed here. For a complete discussion of contact modeling in robotics, readers are referred to Chap. 37.

The three models of greatest interest in grasp analysis are known as *point-contact-without-friction*, *hard-finger*, and *soft-finger* [38.13]. These models select components of the contact twists to transmit between the hand and the object. This is done by equating a subset of the components of the hand and object twist at each contact. The corresponding components of the contact force and moment are also equated, but without regard for the constraints imposed by a friction model (Sect. 38.4.2).

The point-contact-without-friction (PwoF) model is used when the contact patch is very small and the surfaces of the hand and object are slippery. With this model, only the normal component of the translational velocity of the contact point on the hand (i.e., the first component of $\mathbf{v}_{i,\text{hnd}}$) is transmitted to the object. The two components of tangential velocity and the three components of angular velocity are not transmitted. Analogously, the normal component of the contact force is transmitted, but the frictional forces and moments are assumed to be negligible.

A hard finger (HF) model is used when there is significant contact friction, but the contact patch is small, so that no appreciable friction moment exists. When this model is applied to a contact, all three translational velocity components of the contact point on the hand (i.e., the first three components of $\mathbf{v}_{i,\text{hnd}}$) and all three components of the contact force are transmitted through the contact. None of the angular velocity components or moment components are transmitted.

The soft finger (SF) model is used in situations in which the surface friction and the contact patch are large enough to generate significant friction forces and a friction moment about the contact normal. At a contact where this model is enforced, the three translational velocity components of the contact on the hand and the angular velocity component about the contact normal are transmitted (i.e., the first four components of $\mathbf{v}_{i,\text{hnd}}$). Similarly, all three components of contact force

and the normal component of the contact moment are transmitted.

Remark 38.1

The reader may see a contradiction between the rigid-body assumption and the soft-finger model. The rigid-body assumption is an approximation that simplifies all aspects of the analysis of grasping, but nonetheless is sufficiently accurate in many real situations. Without it, grasp analysis would be impractical. On the other hand, the need for a soft-finger model is a clear admission that the finger links and object are not rigid. However, it can be usefully applied in situations in which the amount of deformation required to obtain a large contact patch is small. Such situations occur when the local surface geometries are similar. If large finger or body deformations exist in the real system, the rigid-body approach presented in this chapter should be used with caution.

To develop the PwoF, HF, and SF models, define the relative twist at contact i as follows

$$\begin{pmatrix} \tilde{\mathbf{J}}_i & -\tilde{\mathbf{G}}_i^T \end{pmatrix} \begin{pmatrix} \dot{\mathbf{q}} \\ \mathbf{v} \end{pmatrix} = \mathbf{v}_{i,\text{hnd}} - \mathbf{v}_{i,\text{obj}}.$$

A particular contact model is defined through the matrix $\mathbf{H}_i \in \mathbb{R}^{n_{\lambda_i} \times 6}$, which selects n_{λ_i} components of the relative contact twist and sets them to zero

$$\mathbf{H}_i(\mathbf{v}_{i,\text{hnd}} - \mathbf{v}_{i,\text{obj}}) = \mathbf{0}.$$

These components are referred to as transmitted degrees of freedom (DOF). Define \mathbf{H}_i as follows

$$\mathbf{H}_i = \left[\begin{array}{c|c} \mathbf{H}_{iF} & \mathbf{0} \\ \hline \mathbf{0} & \mathbf{H}_{iM} \end{array} \right], \quad (38.15)$$

where \mathbf{H}_{iF} and \mathbf{H}_{iM} are the translational and rotational component selection matrices. Table 38.2 gives the definitions of the selection matrices for the three contact models, where *vacuous* for \mathbf{H}_{iM} means that the corresponding block row matrix in (38.15) is void (i.e., it has zero rows and columns). Notice that for the SF model, \mathbf{H}_{iM} selects rotation about the contact normal.

After choosing a transmission model for each contact, the kinematic contact constraint equations for all n_c contacts can be written in compact form as

$$\mathbf{H}(\mathbf{v}_{c,\text{hnd}} - \mathbf{v}_{c,\text{obj}}) = \mathbf{0}, \quad (38.16)$$

Table 38.2 Selection matrices for three contact models

Model	n_{λ_i}	\mathbf{H}_{iF}	\mathbf{H}_{iM}
PwoF	1	(1 0 0)	Vacuous
HF	3	$\mathbf{I}_{3 \times 3}$	Vacuous
SF	4	$\mathbf{I}_{3 \times 3}$	(1 0 0)

where

$$\mathbf{H} = \text{Blockdiag}(\mathbf{H}_1, \dots, \mathbf{H}_{n_c}) \in \mathbb{R}^{n_\lambda \times 6n_c},$$

and the number of twist components n_λ transmitted through the n_c contacts is given by $n_\lambda = \sum_{i=1}^{n_c} n_{\lambda i}$.

Finally, by substituting (38.12) and (38.13) into (38.16) one gets the compact form of the velocity kinematic contact constraints

$$(\mathbf{J} \quad -\mathbf{G}^T) \begin{pmatrix} \dot{\mathbf{q}} \\ \mathbf{v} \end{pmatrix} = \mathbf{0}, \quad (38.17)$$

where the grasp matrix and hand Jacobian are finally defined as

$$\begin{aligned} \mathbf{G}^T &= \mathbf{H}\tilde{\mathbf{G}}^T \in \mathbb{R}^{n_\lambda \times 6}, \\ \mathbf{J} &= \mathbf{H}\tilde{\mathbf{J}} \in \mathbb{R}^{n_\lambda \times n_q}. \end{aligned} \quad (38.18)$$

For more details on the construction of \mathbf{H} , the grasp matrix, and the hand Jacobian, readers are referred to [38.14–16] and the references therein. Also, see Example 1, Part 2 and Example 3, Part 2.

It is worth noting that (38.17) can be written in the following form

$$\mathbf{J}\dot{\mathbf{q}} = \mathbf{v}_{\text{cc,hnd}} = \mathbf{v}_{\text{cc,obj}} = \mathbf{G}^T \mathbf{v}, \quad (38.19)$$

where $\mathbf{v}_{\text{cc,hnd}}$ and $\mathbf{v}_{\text{cc,obj}}$ contain only the components of the twists that are transmitted by the contacts. To underline the central role of contact constraints in grasping, it is worth noting that *grasp maintenance* is defined as the situation in which constraints (38.19) are maintained over time. The kinematic contact constraint holds only if the contact force satisfies the friction constraints for the contact models with friction or the unilateral constraint for the contact model without friction (Sect. 38.4.2).

Thus, when a contact is frictionless, contact maintenance implies continued contact, but sliding is allowed. However, when a contact is of the type HF, contact maintenance implies sticking contact, since sliding would violate the HF model. Similarly, for a SF contact, there may be no sliding or relative rotation about the contact normal.

For the remainder of this chapter, it will be assumed that $\mathbf{v}_{\text{cc,hnd}} = \mathbf{v}_{\text{cc,obj}}$, so the notation will be shortened to \mathbf{v}_{cc} .

Planar Simplifications

Assume that the plane of motion is the (x, y) -plane of $\{N\}$. The vectors \mathbf{v} and \mathbf{g} reduce in dimension

from six to three by dropping components three, four, and five. The dimensions of vectors \mathbf{c}_i and \mathbf{p} reduce from three to two. The i -th rotation matrix becomes $\mathbf{R}_i = [\hat{\mathbf{n}}_i \ \hat{\mathbf{t}}_i] \in \mathbb{R}^{2 \times 2}$ (where the third component of $\hat{\mathbf{n}}_i$ and $\hat{\mathbf{t}}_i$ is dropped) and (38.4) holds with $\tilde{\mathbf{R}}_i = \text{Blockdiag}(\mathbf{R}_i, 1) \in \mathbb{R}^{3 \times 3}$. Equation (38.2) holds with

$$\mathbf{P}_i = \begin{pmatrix} \mathbf{I}_{2 \times 2} & \mathbf{0} \\ \mathbf{S}_2(\mathbf{c}_i - \mathbf{p}) & 1 \end{pmatrix},$$

where \mathbf{S}_2 is the analog of the cross product matrix for two-dimensional vectors, given as

$$\mathbf{S}_2(\mathbf{r}) = \begin{pmatrix} -r_y & r_x \end{pmatrix}.$$

Equation (38.7) holds with $\mathbf{d}_{i,j} \in \mathbb{R}^2$ and $\kappa_{i,j} \in \mathbb{R}$ defined as

$$\mathbf{d}_{i,j} = \begin{cases} \mathbf{0}_{2 \times 1} & \text{if contact force } i \text{ does} \\ & \text{not affect the joint } j, \\ \hat{\mathbf{z}}_j & \text{if joint } j \text{ is prismatic,} \\ \mathbf{S}(\mathbf{c}_i - \boldsymbol{\xi}_j)^T & \text{if joint } j \text{ is revolute,} \end{cases}$$

$$\kappa_{i,j} = \begin{cases} 0 & \text{if contact force } i \text{ does} \\ & \text{not affect joint } j, \\ 0 & \text{if joint } j \text{ is prismatic,} \\ 1 & \text{if joint } j \text{ is revolute.} \end{cases}$$

The complete grasp matrix and hand Jacobian have reduced sizes: $\tilde{\mathbf{G}}^T \in \mathbb{R}^{3n_c \times 3}$ and $\tilde{\mathbf{J}} \in \mathbb{R}^{3n_c \times n_q}$. As far as contact constraint is concerned, (38.15) holds with \mathbf{H}_{IF} and \mathbf{H}_{IM} defined in Table 38.3.

In the planar case, the SF and HF models are equivalent, because the object and the hand lie in a plane. Rotations about the contact normals would cause out-of-plane motions. Finally, the dimensions of the grasp matrix and hand Jacobian are reduced to the following sizes: $\mathbf{G}^T \in \mathbb{R}^{n_\lambda \times 3}$ and $\mathbf{J} \in \mathbb{R}^{n_\lambda \times n_q}$. See Example 1, Part 3 and Example 2, Part 1.

38.1.2 Dynamics and Equilibrium

Dynamic equations of the system can be written as

$$\begin{aligned} \mathbf{M}_{\text{hnd}}(\mathbf{q})\ddot{\mathbf{q}} + \mathbf{b}_{\text{hnd}}(\mathbf{q}, \dot{\mathbf{q}}) + \mathbf{J}^T \boldsymbol{\lambda} &= \boldsymbol{\tau}_{\text{app}} \\ \mathbf{M}_{\text{obj}}(\mathbf{u})\ddot{\mathbf{v}} + \mathbf{b}_{\text{obj}}(\mathbf{u}, \mathbf{v}) - \mathbf{G}\boldsymbol{\lambda} &= \mathbf{g}_{\text{app}} \end{aligned} \quad (38.20)$$

subject to constraint (38.17),

Table 38.3 Definitions

Model	$n_{\lambda i}$	\mathbf{H}_{IF}	\mathbf{H}_{IM}
PwoF	1	$\begin{pmatrix} 1 & 0 \end{pmatrix}$	Vacuous
HF/SF	2	$\mathbf{I}_{2 \times 2}$	Vacuous

Table 38.4 Vectors of contact force and moment components, also known as the wrench intensity vector, transmitted through contact i

Model	λ_i
PwoF	(f_{in})
HF	$(f_{in} f_{it} f_{io})^T$
SF	$(f_{in} f_{it} f_{io} m_{in})^T$

where $\mathbf{M}_{\text{hnd}}(\cdot)$ and $\mathbf{M}_{\text{obj}}(\cdot)$ are symmetric, positive definite inertia matrices, $\mathbf{b}_{\text{hnd}}(\cdot, \cdot)$ and $\mathbf{b}_{\text{obj}}(\cdot, \cdot)$ are the velocity-product terms, \mathbf{g}_{app} is the force and moment applied to the object by gravity and other external sources, $\boldsymbol{\tau}_{\text{app}}$ is the vector of external loads and actuator actions, and the vector $\mathbf{G}\boldsymbol{\lambda}$ is the total wrench applied to the object by the hand. The vector $\boldsymbol{\lambda}$ contains the contact force and moment components transmitted through the contacts and expressed in the contact frames. Specifically, $\boldsymbol{\lambda} = [\lambda_1^T \cdots \lambda_{n_c}^T]^T$, where

$$\lambda_i = \mathbf{H}_i [f_{in} f_{it} f_{io} m_{in} m_{it} m_{io}]^T.$$

The subscripts indicate one normal (n) and two tangential (t,o) components of contact force \mathbf{f} and moment \mathbf{m} . For a SF, HF, or PwoF contact, λ_i is defined as in Table 38.4. Finally, it is worth noting that $\mathbf{G}_i \lambda_i = \tilde{\mathbf{G}}_i \mathbf{H}_i^T \lambda_i$ is the wrench applied through contact i , where $\tilde{\mathbf{G}}_i$ and \mathbf{H}_i are defined in (38.6) and (38.15). The vector λ_i is known as the wrench intensity vector for contact i .

Equation (38.20) represents the dynamics of the hand and object without regard for the kinematic constraints imposed by the contact models. Enforcing them, the dynamic model of the system can be written as follows

$$\begin{pmatrix} \mathbf{J}^T \\ -\mathbf{G} \end{pmatrix} \boldsymbol{\lambda} = \begin{pmatrix} \boldsymbol{\tau} \\ \mathbf{g} \end{pmatrix} \quad (38.21)$$

38.2 Controllable Twists and Wrenches

In hand design and in grasp and manipulation planning, it is important to know the set of twists that can be imparted to the object by movements of the fingers, and conversely, the conditions under which the hand can prevent all possible motions of the object. The dual view is that one needs to know the set of wrenches that the hand can apply to the object and under what conditions any wrench in \mathbb{R}^6 can be applied through the contacts. This knowledge will be gained by studying the various subspaces associated with \mathbf{G} and \mathbf{J} [38.17].

The spaces, shown in Fig. 38.3, are the column spaces and null spaces of \mathbf{G} , \mathbf{G}^T , \mathbf{J} , and \mathbf{J}^T . Column

subject to $\mathbf{J}\dot{\mathbf{q}} = \mathbf{G}^T \mathbf{v} = \mathbf{v}_{\text{cc}}$, where

$$\begin{aligned} \boldsymbol{\tau} &= \boldsymbol{\tau}_{\text{app}} - \mathbf{M}_{\text{hnd}}(\mathbf{q})\ddot{\mathbf{q}} - \mathbf{b}_{\text{hnd}}(\mathbf{q}, \dot{\mathbf{q}}) \\ \mathbf{g} &= \mathbf{g}_{\text{app}} - \mathbf{M}_{\text{obj}}(\mathbf{u})\dot{\mathbf{v}} - \mathbf{b}_{\text{obj}}(\mathbf{u}, \mathbf{v}). \end{aligned} \quad (38.22)$$

One should notice that the dynamic equations are closely related to the velocity kinematic model in (38.17). Specifically, just as \mathbf{J} and \mathbf{G}^T transmit only selected components of contact twists, \mathbf{J}^T and \mathbf{G} in (38.20) serve to transmit only the corresponding components of the contact wrenches.

When the inertia terms are negligible, as occurs during slow motion, the system is said to be quasi-static. In this case, (38.22) becomes

$$\begin{aligned} \boldsymbol{\tau} &= \boldsymbol{\tau}_{\text{app}}, \\ \mathbf{g} &= \mathbf{g}_{\text{app}}, \end{aligned} \quad (38.23)$$

and does not depend on joint and object velocities. Consequently, when the grasp is in static equilibrium or moves quasi-statically, one can solve the first equation and the constraint in (38.21) independently to compute $\boldsymbol{\lambda}$, $\dot{\mathbf{q}}$, and \mathbf{v} . It is worth noting that such a force/velocity decoupled solution is not possible when dynamic effects are appreciable, since the first equation in (38.21) depends on the third one through (38.22).

Remark 38.2

Equation (38.21) highlights an important alternative view of the grasp matrix and the hand Jacobian. \mathbf{G} can be thought of as a mapping from the transmitted contact forces and moments to the set of wrenches that the hand can apply to the object, while \mathbf{J}^T can be thought of as a mapping from the transmitted contact forces and moments to the vector of joint loads. Notice that these interpretations hold for both dynamic and quasi-static conditions.

space (also known as range) and null space will be denoted by $\mathcal{R}(\cdot)$ and $\mathcal{N}(\cdot)$, respectively. The arrows show the propagation of the various velocity and load quantities through the grasping system. For example, in the left part of Fig. 38.3 it is shown how any vector $\dot{\mathbf{q}} \in \mathbb{R}^{n_q}$ can be decomposed into a sum of two orthogonal vectors in $\mathcal{R}(\mathbf{J}^T)$ and in $\mathcal{N}(\mathbf{J})$ and how $\dot{\mathbf{q}}$ is mapped to $\mathcal{R}(\mathbf{J})$ by multiplication by \mathbf{J} .

It is important to recall two facts from linear algebra. First, a matrix \mathbf{A} maps vectors from $\mathcal{R}(\mathbf{A}^T)$ to $\mathcal{R}(\mathbf{A})$ in a one-to-one and onto fashion, that is, the map \mathbf{A} is a bijection. The generalized inverse \mathbf{A}^+ of

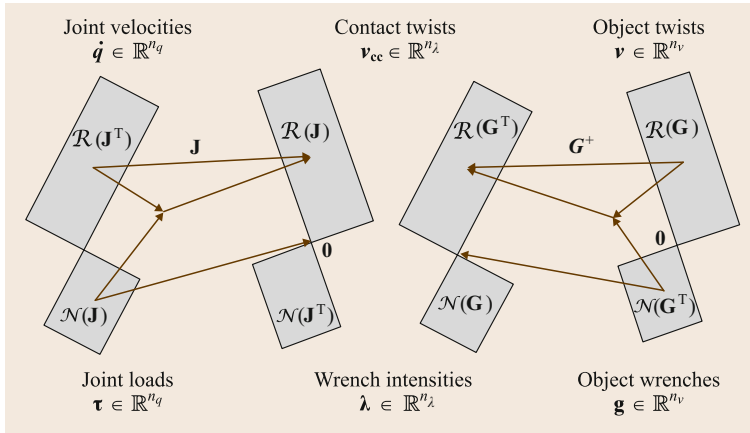


Fig. 38.3 Linear maps relating twists and wrenches of a grasping system

\mathbf{A} is a bijection that maps vectors in the opposite direction [38.18]. Also, \mathbf{A} maps all vectors in $\mathcal{N}(\mathbf{A})$ to zero. Finally, there is no non-trivial vector that \mathbf{A} can map into $\mathcal{N}(\mathbf{A}^T)$. This implies that if $\mathcal{N}(\mathbf{G}^T)$ is non-trivial, then the hand will not be able to control all degrees of freedom of the object’s motion. This is certainly true for quasi-static grasping, but when dynamics are important, they may cause the object to move along the directions in $\mathcal{N}(\mathbf{G}^T)$.

38.2.1 Grasp Classifications

The four null spaces motivate a basic classification of grasping systems defined in Table 38.5. Assuming solutions to (38.21) exist, the following force and velocity equations provide insight into the physical meaning of the various null spaces

$$\dot{\mathbf{q}} = \mathbf{J}^+ \mathbf{v}_{cc} + \mathbf{N}(\mathbf{J}) \boldsymbol{\gamma}, \tag{38.24}$$

$$\mathbf{v} = (\mathbf{G}^T)^+ \mathbf{v}_{cc} + \mathbf{N}(\mathbf{G}^T) \boldsymbol{\gamma}, \tag{38.25}$$

$$\boldsymbol{\lambda} = -\mathbf{G}^+ \mathbf{g} + \mathbf{N}(\mathbf{G}) \boldsymbol{\gamma}, \tag{38.26}$$

$$\boldsymbol{\lambda} = (\mathbf{J}^T)^+ \boldsymbol{\tau} + \mathbf{N}(\mathbf{J}^T) \boldsymbol{\gamma}. \tag{38.27}$$

In these equations, \mathbf{A}^+ denotes the generalized inverse, henceforth pseudoinverse, of a matrix \mathbf{A} , $\mathbf{N}(\mathbf{A})$ denotes

a matrix whose columns form a basis for $\mathcal{N}(\mathbf{A})$, and $\boldsymbol{\gamma}$ is an arbitrary vector of appropriate dimension that parameterizes the solution sets. If not otherwise specified, the context will make clear if the generalized inverse is left or right.

If the null spaces represented in the equations are non-trivial, then one immediately sees the first many-to-one mapping in Table 38.5. To see the other many-to-one mappings, and in particular the defective class, consider (38.24). It can be rewritten with \mathbf{v}_{cc} decomposed into orthogonal components \mathbf{v}_{rs} and \mathbf{v}_{lns} in $\mathcal{R}(\mathbf{J})$ and $\mathcal{N}(\mathbf{J}^T)$, respectively

$$\dot{\mathbf{q}} = \mathbf{J}^+ (\mathbf{v}_{rs} + \mathbf{v}_{lns}) + \mathbf{N}(\mathbf{J}) \boldsymbol{\gamma}. \tag{38.28}$$

Recall that every vector in $\mathcal{N}(\mathbf{A}^T)$ is orthogonal to every row of \mathbf{A}^+ . Therefore $\mathbf{J}^+ \mathbf{v}_{lns} = \mathbf{0}$. If $\boldsymbol{\gamma}$ and \mathbf{v}_{rs} are fixed in (38.28), then $\dot{\mathbf{q}}$ is unique. Thus it is clear that if $\mathcal{N}(\mathbf{J}^T)$ is non-trivial, then a subspace of twists of the hand at the contacts will map to a single joint velocity vector. Applying the same approach to the other three equations (38.25)–(38.27) yields the other many-to-one mappings listed in Table 38.5.

Equations (38.21) and (38.24)–(38.27), motivate the following definitions.

Definition 38.1 Redundant

A grasping system is said to be *redundant* if $\mathcal{N}(\mathbf{J})$ is non-trivial.

Joint velocities $\dot{\mathbf{q}}$ in $\mathcal{N}(\mathbf{J})$ are referred to as *internal hand velocities*, since they correspond to finger motions, but do not generate motion of the hand in the constrained directions at the contact points. If the quasi-static model applies, it can be shown that these motions are not influenced by the motion of the object and vice versa.

Table 38.5 Basic grasp classes

Condition	Class	Many-to-one
$\mathcal{N}(\mathbf{J}) \neq \mathbf{0}$	Redundant	$\dot{\mathbf{q}} \rightarrow \mathbf{v}_{cc}$ $\boldsymbol{\tau} \rightarrow \boldsymbol{\lambda}$
$\mathcal{N}(\mathbf{G}^T) \neq \mathbf{0}$	Indeterminate	$\mathbf{v} \rightarrow \mathbf{v}_{cc}$ $\mathbf{g} \rightarrow \boldsymbol{\lambda}$
$\mathcal{N}(\mathbf{G}) \neq \mathbf{0}$	Graspable	$\boldsymbol{\lambda} \rightarrow \mathbf{g}$ $\mathbf{v}_{cc} \rightarrow \mathbf{v}$
$\mathcal{N}(\mathbf{J}^T) \neq \mathbf{0}$	Defective	$\boldsymbol{\lambda} \rightarrow \boldsymbol{\tau}$ $\mathbf{v}_{cc} \rightarrow \dot{\mathbf{q}}$

Definition 38.2 Indeterminate

A grasping system is said to be *indeterminate* if $\mathcal{N}(\mathbf{G}^T)$ is non-trivial.

Object twists \mathbf{v} in $\mathcal{N}(\mathbf{G}^T)$ are called *internal object twists*, since they correspond to motions of the object, but do not cause motion of the object in the constrained directions at the contacts. If the static model applies, it can be shown that these twists cannot be controlled by finger motions.

Definition 38.3 Graspable

A grasping system is said to be *graspable* if $\mathcal{N}(\mathbf{G})$ is non-trivial.

Wrench intensities $\boldsymbol{\lambda}$ in $\mathcal{N}(\mathbf{G})$ are referred to as *internal object forces*. These wrenches are *internal* because they do not contribute to the acceleration of the object, i. e., $\mathbf{G}\boldsymbol{\lambda} = \mathbf{0}$. Instead, these wrench intensities affect the tightness of the grasp. Thus, internal wrench intensities play a fundamental role in maintaining grasps that rely on friction (Sect. 38.4.2).

Definition 38.4 Defective

A grasping system is said to be *defective* if $\mathcal{N}(\mathbf{J}^T)$ is non-trivial.

Wrench intensities $\boldsymbol{\lambda}$ in $\mathcal{N}(\mathbf{J}^T)$ are called *internal hand forces*. These forces do not influence the hand joint dynamics given in (38.20). If the static model is considered, it can be easily shown that wrench intensities belonging to $\mathcal{N}(\mathbf{J}^T)$ cannot be generated by joint actions, but can be resisted by the structure of the hand.

See Example 1, Part 4, Example 2, Part 2 and Example 3, Part 3.

38.2.2 Limitations of Rigid-Body Formulation

The rigid-body dynamics equation (38.20) can be rewritten with Lagrange multipliers associated with the contact constraints as

$$\mathbf{M}_{\text{dyn}} \begin{pmatrix} \ddot{\mathbf{q}} \\ \dot{\mathbf{v}} \\ \boldsymbol{\lambda} \end{pmatrix} = \begin{pmatrix} \boldsymbol{\tau} - \mathbf{b}_{\text{hnd}} \\ \mathbf{v} - \mathbf{b}_{\text{obj}} \\ \mathbf{b}_c \end{pmatrix}, \quad (38.29)$$

where $\mathbf{b}_c = [\partial(\mathbf{J}\dot{\mathbf{q}})/\partial\mathbf{q}]\dot{\mathbf{q}} - [\partial(\mathbf{G}\mathbf{v})/\partial\mathbf{u}]\dot{\mathbf{u}}$ and

$$\mathbf{M}_{\text{dyn}} = \begin{pmatrix} \mathbf{M}_{\text{hnd}} & \mathbf{0} & \mathbf{J}^T \\ \mathbf{0} & \mathbf{M}_{\text{obj}} & -\mathbf{G} \\ \mathbf{J} & -\mathbf{G}^T & \mathbf{0} \end{pmatrix}.$$

In order for this equation to completely determine the motion of the system, it is necessary that matrix \mathbf{M}_{dyn} be invertible. This case is considered in detail in [38.19], where the dynamics of multi-finger manipulation is studied under the hypothesis that the hand Jacobian is full row rank, i. e., $\mathcal{N}(\mathbf{J}^T) = \mathbf{0}$. For all manipulation systems with non-invertible \mathbf{M}_{dyn} , rigid-body dynamics fails to determine the motion and the wrench intensity vector. By observing that

$$\begin{aligned} \mathcal{N}(\mathbf{M}_{\text{dyn}}) \\ = \{(\ddot{\mathbf{q}}, \dot{\mathbf{v}}, \boldsymbol{\lambda})^T | \ddot{\mathbf{q}} = \mathbf{0}, \dot{\mathbf{v}} = \mathbf{0}, \boldsymbol{\lambda} \in \mathcal{N}(\mathbf{J}^T) \cap \mathcal{N}(\mathbf{G})\}, \end{aligned}$$

the same arguments apply under quasi-static conditions defined by (38.21) and (38.23). When $\mathcal{N}(\mathbf{J}^T) \cap \mathcal{N}(\mathbf{G}) \neq \mathbf{0}$, the rigid-body approach fails to solve the first equation in (38.21), thus leaving $\boldsymbol{\lambda}$ indeterminate.

Definition 38.5 Hyperstatic

A grasping system is said to be *hyperstatic* if

$$\mathcal{N}(\mathbf{J}^T) \cap \mathcal{N}(\mathbf{G})$$

is non-trivial.

In such systems there are internal forces (Definition 38.3) belonging to $\mathcal{N}(\mathbf{J}^T)$ that are not controllable as discussed for defective grasps. Rigid-body dynamics is not satisfactory for hyperstatic grasps, since the rigid-body assumption leads to undetermined contact wrenches [38.20].

See Example 3, Part 3.

38.2.3 Desirable Properties

For a general purpose grasping system, there are three main desirable properties: control of the object twist \mathbf{v} , control of object wrench \mathbf{g} , and control of the internal forces. Control of these quantities implies that the hand can deliver the desired \mathbf{v} and \mathbf{g} with specified grip pressure by the appropriate choice of joint velocities and actions. The conditions on \mathbf{J} and \mathbf{G} equivalent to these properties are given in Table 38.6.

We derive the conditions in two steps. First, we ignore the structure and configuration of the hand (captured in \mathbf{J}) by assuming that each contact point on each

Table 38.6 Desirable properties of a grasp

Task requirement	Required conditions
All wrenches possible, \mathbf{g} } All twists possible, \mathbf{v} }	$\text{rank}(\mathbf{G}) = n_v$
Control all wrenches, \mathbf{g} } Control all twists, \mathbf{v} }	$\text{rank}(\mathbf{G}\mathbf{J}) = \text{rank}(\mathbf{G}) = n_v$
Control all internal forces	$\mathcal{N}(\mathbf{G}) \cap \mathcal{N}(\mathbf{J}^T) = \mathbf{0}$



Fig. 38.4 The Salisbury Hand

finger can be commanded to move in any direction transmitted by the chosen contact model. An important perspective here is that \mathbf{v}_{cc} is seen as the independent input variable and \mathbf{v} is seen as the output. The dual interpretation is that the actuators can generate any contact force and moment in the constrained directions at each contact. Similarly, λ is seen as the input and \mathbf{g} is seen as the output. The primary property of interest under this assumption is whether or not the arrangement and types of contacts on the object (captured in \mathbf{G}) are such that a sufficiently dexterous hand could control its fingers so as to impart any twist $\mathbf{v} \in \mathbb{R}^6$ to the object and, similarly, to apply any wrench $\mathbf{g} \in \mathbb{R}^6$ to the object.

All Object Twists Possible

Given a set of contact locations and types, by solving (38.19) for \mathbf{v} or observing the map \mathbf{G} on the right side of Fig. 38.3, one sees that the achievable object twists are those in $\mathcal{R}(\mathbf{G})$. Those in $\mathcal{N}(\mathbf{G}^T)$ cannot be achieved by any hand using the given grasp. Therefore, to achieve any object twist, we must have: $\mathcal{N}(\mathbf{G}^T) = \mathbf{0}$, or equivalently, $\text{rank}(\mathbf{G}) = n_v$. Any grasp with three non-collinear hard contacts or two distinct soft contacts satisfies this condition.

All Object Wrenches Possible

This case is the dual of the previous case, so we expect the same condition. From (38.21), one immediately obtains the condition $\mathcal{N}(\mathbf{G}^T) = \mathbf{0}$, so again we have $\text{rank}(\mathbf{G}) = n_v$.

To obtain the conditions needed to control the various quantities of interest, the structure of the hand

cannot be ignored. Recall that the only achievable contact twists on the hand are in $\mathcal{R}(\mathbf{J})$, which is not necessarily equal to \mathbb{R}^{n_λ} .

Control All Object Twists

By solving (38.17) for \mathbf{v} , one sees that in order to cause any object twist \mathbf{v} by choice of joint velocities $\dot{\mathbf{q}}$, we must have $\mathcal{R}(\mathbf{G}\mathbf{J}) = \mathbb{R}^{n_v}$ and $\mathcal{N}(\mathbf{G}^T) = \mathbf{0}$. These conditions are equivalent to $\text{rank}(\mathbf{G}\mathbf{J}) = \text{rank}(\mathbf{G}) = n_v$.

Control All Object Wrenches

This property is dual to the previous one. Analysis of (38.21) yields the same conditions:

$$\text{rank}(\mathbf{G}\mathbf{J}) = \text{rank}(\mathbf{G}) = n_v.$$

Control All Internal Forces

Equation (38.20) shows that wrench intensities with no effect on object motion are those in $\mathcal{N}(\mathbf{G})$. In general, not all the internal forces may be actively controlled by joint actions. In [38.16, 21] it has been shown that all internal forces in $\mathcal{N}(\mathbf{G})$ are controllable if and only if $\mathcal{N}(\mathbf{G}) \cap \mathcal{N}(\mathbf{J}^T) = \mathbf{0}$.

See Example 1, Part 5 and Example 2, Part 3.

Design Considerations of the Salisbury Hand

The Salisbury Hand in Fig. 38.4 was designed to have the smallest number of joints that would meet all the task requirements in Table 38.6. Assuming HF contacts, three non-collinear contacts is the minimum number such that $\text{rank}(\mathbf{G}) = n_v = 6$. In this case, \mathbf{G} has six rows and nine columns and the dimension of $\mathcal{N}(\mathbf{G})$ is three [38.2, 8]. The ability to control all internal forces and apply an arbitrary wrench to the object requires that $\mathcal{N}(\mathbf{G}) \cap \mathcal{N}(\mathbf{J}^T) = \mathbf{0}$, so the minimum dimension of the column space of \mathbf{J} is nine. To achieve this, the hand must have at least nine joints, which Salisbury implemented as three fingers, each with three revolute joints.

The intended way to execute a dexterous manipulation task with the Salisbury Hand is to grasp the object at three non-collinear points with the fingertips, forming a grasp triangle. To secure the grasp, the internal forces are controlled so that the contact points are maintained without sliding. Dexterous manipulation can be thought of as moving the fingertips to control the positions of the vertices of the grasp triangle.

38.3 Compliant Grasps

In this section we extend the rigid-body model to include compliance. This is needed to design controllers that can implement desired compliance behaviors of a grasped object when it contacts the environment, which can increase the robustness of static grasps and dexterous manipulation tasks. It also facilitates the analysis of hands designed with flexible mechanical elements [38.22, 23] and grasp control strategies that exploit grasp *synergies* [38.24, 25]. Thanks to compliance, hands can be designed to maintain a secure grasp with fewer joints, which provides greater mechanical robustness and reduces the complexity of planning grasps.

On the other hand, reducing the number of DOFs in robotic hands demands a compliant design of the whole structure to adapt the shape of the hand to different objects and to improve robustness with respect to uncertainties [38.26]. Compliance can be passive or active. Passive compliance is due to the structural deformation of robot components, including joints, while active compliance refers to virtual elasticity of actuators, e.g., due to the proportional action of a PD joint controller, that can be actively set by changing the control parameters [38.26–29].

In the following, we extend the grasp analysis relaxing the rigid-body contact constraints to take into account both the compliance and the low number of DOFs in robotic hands.

If the hand structure is not perfectly stiff, as shown in Fig. 38.5, the actual vector of joint variables \mathbf{q} can be different from the reference one \mathbf{q}_r , given to the joint actuator controllers, and their difference is related to the joint effort $\boldsymbol{\tau}$ through a compliance matrix $\mathbf{C}_q \in \mathbb{R}^{n_q \times n_q}$ by the constitutive equation

$$\mathbf{q}_r - \mathbf{q} = \mathbf{C}_q \boldsymbol{\tau} . \quad (38.30)$$

Note that if the hand structure is perfectly rigid, $\mathbf{C}_q = 0$ and the hand stiffness $\mathbf{K}_q = \mathbf{C}_q^{-1}$ is not defined.

It will be clear in a moment that to deal with a low number of DOFs of the hand, a compliant model of the contact must be considered. According to Definition 38.4, in case of a low number of DOFs, it is very likely that the grasp will be defective, i.e., with a non-trivial $\mathcal{N}(\mathbf{J}^1)$. It is worth noting that this typically happens also in power grasps [38.30] where the hand envelops the object establishing contacts even with inner limbs. In this case the hand Jacobian is a tall matrix with a non-trivial null space of its transpose.

If the system is very defective, it is very likely that the grasp will be hyperstatic according to Def-

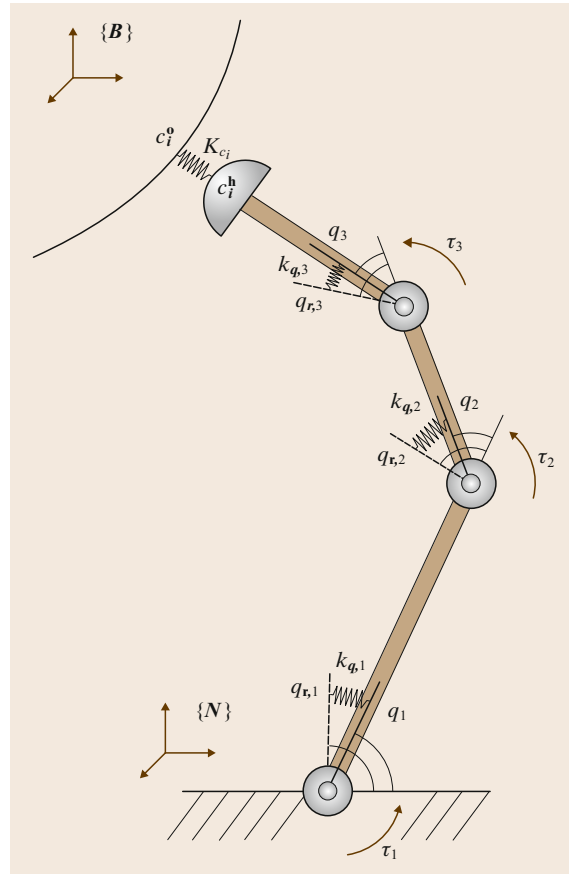


Fig. 38.5 Compliant joints and compliant contacts, main definitions

inition 38.5 and consequently the rigid-body model in (38.21) is under-determined and does not admit a unique solution for the contact force vector $\boldsymbol{\lambda}$ as discussed in Sect. 38.2.2. Note that computing the force distribution $\boldsymbol{\lambda}$ is crucial in grasp analysis since it allows one to evaluate if the contact constraints are fulfilled, and consequently, if the grasp will be maintained.

The force distribution problem in hyperstatic grasps is an under-determined problem of statics under the assumption of rigid contacts of (38.17). To solve the problem, we need to enrich the model with more information on the contact forces. A possible solution is to substitute the rigid-body kinematic constraint (38.19) with a compliant model of the contact interaction [38.21], obtained introducing a set of springs between the contact points on the hand \mathbf{c}^h and on the object \mathbf{c}^o as shown in Fig. 38.5

$$\mathbf{C}_c \boldsymbol{\lambda} = \mathbf{c}^h - \mathbf{c}^o , \quad (38.31)$$

where $\mathbf{C}_c \in \mathbb{R}^{n_\lambda \times n_\lambda}$ is the contact compliance matrix which is symmetric and positive definite. The contact stiffness matrix is defined as the reciprocal of the contact compliance matrix $\mathbf{K}_c = \mathbf{C}_c^{-1}$.

The analysis is presented in a quasi-static framework: from an equilibrium reference configuration $\mathbf{q}_{r,0}$, \mathbf{q}_0 , $\boldsymbol{\tau}_0$, $\boldsymbol{\lambda}_0$, \mathbf{u}_0 and \mathbf{g}_0 , a small input perturbation is applied to the joint references $\mathbf{q}_{r,0} + \Delta\mathbf{q}_r$ and to the external load $\mathbf{g}_0 + \Delta\mathbf{g}$ which moves the grasp system to a new equilibrium configuration whose linear approximation is represented by $\mathbf{q}_0 + \Delta\mathbf{q}$, $\boldsymbol{\tau}_0 + \Delta\boldsymbol{\tau}$, $\boldsymbol{\lambda}_0 + \Delta\boldsymbol{\lambda}$, $\mathbf{u}_0 + \Delta\mathbf{u}$.

In the following, for the sake of simplicity, it is convenient to refer \mathbf{G} and \mathbf{J} matrices to the object reference frame $\{\mathbf{B}\}$ and not to the inertial frame $\{\mathbf{N}\}$ as previously described. Note that this only applies to this section on compliance analysis, while the rest of this chapter still refers to matrices \mathbf{G} and \mathbf{J} as described in Sect. 38.1.1.

Let $\mathbf{R}_b \in \mathbb{R}^{3 \times 3}$ represent the orientation of the object frame $\{\mathbf{B}\}$ with respect to the inertial frame. Then the object twist referred to $\{\mathbf{B}\}$ is given as

$$\mathbf{v}_{i,\text{obj}} = \bar{\mathbf{R}}_b^T \begin{pmatrix} \mathbf{v}_{i,\text{obj}}^{\mathbf{N}} \\ \boldsymbol{\omega}_{\text{obj}}^{\mathbf{N}} \end{pmatrix}, \quad (38.32)$$

where

$$\bar{\mathbf{R}}_b = \text{Blockdiag}(\mathbf{R}_b, \mathbf{R}_b) = \begin{pmatrix} \mathbf{R}_b & \mathbf{0} \\ \mathbf{0} & \mathbf{R}_b \end{pmatrix} \in \mathbb{R}^{6 \times 6}.$$

Then, substituting $\mathbf{P}_i^T \mathbf{v}$ from (38.2) into (38.32) yields the partial grasp matrix $\bar{\mathbf{G}}_i^T \in \mathbb{R}^{6 \times 6}$, that maps the object twist from $\{\mathbf{N}\}$ to contact frame $\{\mathbf{C}\}_i$ referred to $\{\mathbf{B}\}$.

Similarly, the hand twists can be expressed to the object frame $\{\mathbf{B}\}$

$$\mathbf{v}_{i,\text{hnd}} = \bar{\mathbf{R}}_b^T \begin{pmatrix} \mathbf{v}_{i,\text{hnd}}^{\mathbf{N}} \\ \boldsymbol{\omega}_{i,\text{hnd}}^{\mathbf{N}} \end{pmatrix} \quad (38.33)$$

and combining (38.33) and (38.7) yields the partial hand Jacobian $\bar{\mathbf{J}}_i \in \mathbb{R}^{6 \times n_q}$, which relates the joint velocities to the contact twists on the hand expressed with respect to $\{\mathbf{B}\}$.

Table 38.7 gives the definitions of the selection matrices for the three contact models when object and hand twists are referred to frame $\{\mathbf{B}\}$. In the planar case, as far as contact constraint is concerned, equation (38.15) holds with \mathbf{H}_{iF} and \mathbf{H}_{iM} defined in Table 38.8.

The contact force variation $\Delta\boldsymbol{\lambda}$ from the equilibrium configuration is then related to the relative displacement between the object and the fingers at the contact points as

$$\mathbf{C}_c \Delta\boldsymbol{\lambda} = (\mathbf{J} \Delta\mathbf{q} - \mathbf{G}^T \Delta\mathbf{u}). \quad (38.34)$$

Table 38.7 Selection matrices for three contact models, when the object twists are expressed with respect to $\{\mathbf{B}\}$

Model	n_{λ_i}	\mathbf{H}_{iF}	\mathbf{H}_{iM}
PwoF	1	$\hat{\mathbf{n}}_i^{bT}$	Vacuous
HF	3	$[\hat{\mathbf{n}}_i^b, \hat{\boldsymbol{\tau}}_i^b, \hat{\boldsymbol{\sigma}}_i^b]^T$	Vacuous
SF	4	$[\hat{\mathbf{n}}_i^b, \hat{\boldsymbol{\tau}}_i^b, \hat{\boldsymbol{\sigma}}_i^b]^T$	$\hat{\mathbf{n}}_i^{bT}$

$\hat{\mathbf{n}}_i^b$ is the normal unit vector at the contact i expressed with respect to $\{\mathbf{B}\}$ reference system.

Table 38.8 Selection matrices for the planar simplified case, when the object twists are expressed with respect to $\{\mathbf{B}\}$

Model	n_{λ_i}	\mathbf{H}_{iF}	\mathbf{H}_{iM}
PwoF	1	$\hat{\mathbf{n}}_i^{bT}$	Vacuous
HF/SF	2	$[\hat{\mathbf{n}}_i^b, \hat{\boldsymbol{\tau}}_i^b]^T$	Vacuous

By assuming that the perturbed configuration is sufficiently near to the reference one, the following linearized relationships can be found for \mathbf{g} , and $\boldsymbol{\tau}$

$$\Delta\mathbf{g} = -\mathbf{G} \Delta\boldsymbol{\lambda} \quad (38.35)$$

$$\Delta\boldsymbol{\tau} = \mathbf{J}^T \Delta\boldsymbol{\lambda} + \mathbf{K}_{J,q} \Delta\mathbf{q} + \mathbf{K}_{J,u} \Delta\mathbf{u} \quad (38.36)$$

where

$$\mathbf{K}_{J,q} = \frac{\partial \mathbf{J} \boldsymbol{\lambda}_0}{\partial \mathbf{q}} \quad \text{and} \quad \mathbf{K}_{J,u} = \frac{\partial \mathbf{J} \boldsymbol{\lambda}_0}{\partial \mathbf{u}}$$

are the variation of the hand Jacobian with respect to \mathbf{q} and \mathbf{u} variations, respectively.

Remark 38.3

In (38.35) and (38.36) both the grasp matrix and hand Jacobian are expressed with respect to the object reference frame, and by neglecting rolling between the fingers and the object at the contact points, \mathbf{G} becomes constant, while $\mathbf{J}(\mathbf{q}, \mathbf{u})$, in general, depends on both hand and object configurations. Matrix $\mathbf{K}_{J,q}$ represent the variability of $\mathbf{J}(\mathbf{q}, \mathbf{u})$ matrix with respect to hand and object configurations.

Matrices $\mathbf{K}_{J,q} \in \mathbb{R}^{n_q \times n_q}$ and $\mathbf{K}_{J,u} \in \mathbb{R}^{n_q \times n_v}$ are usually referred to as *geometric stiffness matrices* [38.28]. Furthermore, it can be verified that the matrix $\mathbf{K}_{J,q}$ is symmetric [38.27].

By substituting (38.36) in (38.30) we get

$$\mathbf{J}_R \mathbf{C}_q \mathbf{J}^T \Delta\boldsymbol{\lambda} = \mathbf{J}_R \Delta\mathbf{q}_r - \mathbf{J} \Delta\mathbf{q} - \mathbf{J}_R \mathbf{C}_q \mathbf{K}_{J,u} \Delta\mathbf{u}, \quad (38.37)$$

where

$$\mathbf{J}_R = \mathbf{J} (\mathbf{I} + \mathbf{C}_q \mathbf{K}_{J,q})^{-1}.$$

Summing (38.34) and (38.37) the following expression can be found for the contact forces displacement $\Delta\lambda$

$$\Delta\lambda = \mathbf{K}_{c,e} (\mathbf{J}_R \Delta\mathbf{q}_r - \mathbf{G}_R^T \Delta\mathbf{u}) \quad (38.38)$$

where

$$\mathbf{G}_R^T = \mathbf{G}^T + \mathbf{J}_R \mathbf{C}_q \mathbf{K}_{J,u}$$

and

$$\mathbf{K}_{c,e} = (\mathbf{C}_c + \mathbf{J}_R \mathbf{C}_q \mathbf{J}^T)^{-1}. \quad (38.39)$$

Matrix $\mathbf{K}_{c,e}$ represents the equivalent contact stiffness, that takes into account both the joint and the contact compliance. If the geometrical terms are neglected, i. e., $\mathbf{K}_{J,q} = 0$ and $\mathbf{K}_{J,u} = 0$, the classical expression $\mathbf{K}_{c,e} = (\mathbf{C}_c + \mathbf{J} \mathbf{C}_q \mathbf{J}^T)^{-1}$ for the equivalent contact stiffness matrix can be found [38.28].

By substituting (38.38) in (38.35), the object displacement can be evaluated as a function of the small input perturbations $\Delta\mathbf{q}_r$ and $\Delta\mathbf{g}$

$$\Delta\mathbf{u} = (\mathbf{G} \mathbf{K}_{c,e} \mathbf{G}_R^T)^{-1} (\mathbf{G} \mathbf{K}_{c,e} \mathbf{J}_R \Delta\mathbf{q}_r + \Delta\mathbf{g}). \quad (38.40)$$

When $\Delta\mathbf{q}_r = 0$, (38.40) can be rewritten as

$$\Delta\mathbf{g} = \mathbf{K} \Delta\mathbf{u},$$

$$\text{with } \mathbf{K} = \mathbf{G} \mathbf{K}_{c,e} \mathbf{G}_R^T,$$

where the term that multiplies the external wrench variation $\Delta\mathbf{g}$ represents the reciprocal of the *grasp stiffness matrix* \mathbf{K} . The grasp stiffness evaluates ability of the

38.4 Restraint Analysis

The most fundamental requirements in grasping and dexterous manipulation are the abilities to hold an object and control its position and orientation relative to the palm of the hand. The two most useful characterizations of grasp restraint are *force closure* and *form closure*. These names were in use as early as 1876 in the field of machine design to distinguish between joints that required an external force to maintain contact, and those that did not [38.31]. For example, some water wheels had a cylindrical axle that was laid in a horizontal semi-cylindrical groove split on either side of the wheel. During operation, the weight of the wheel acted to *close* the groove-axle contacts, hence the term *force closure*. By contrast, if the grooves were replaced by cylindrical holes just long enough to accept the axle, then the contacts would be closed by the geometry (even if the direction of the gravitational force was reversed), hence the term *form closure*.

robotic grasp to resist to external load variations applied to the object.

Regarding the force distribution $\Delta\lambda$, by substituting (38.40) into (38.38), the variation of the contact forces is evaluated as

$$\Delta\lambda = \mathbf{G}_g^+ \Delta\mathbf{g} + \mathbf{P} \Delta\mathbf{q}_r, \quad (38.41)$$

where

$$\mathbf{G}_g^+ = \mathbf{K}_{c,e} \mathbf{G}_R^T (\mathbf{G} \mathbf{K}_{c,e} \mathbf{G}_R^T)^{-1},$$

$$\mathbf{P} = (\mathbf{I} - \mathbf{G}_g^+ \mathbf{G}) \mathbf{K}_{c,e} \mathbf{J}_R.$$

Matrix \mathbf{G}_g^+ is a right pseudo-inverse of grasp matrix \mathbf{G} that takes into account both the geometrical effects and the hand and contact stiffness. Matrix \mathbf{P} maps the reference joint variables $\Delta\mathbf{q}_r$ to the contact force variation $\Delta\lambda$.

It is worth noting that $(\mathbf{I} - \mathbf{G}_g^+ \mathbf{G})$ is a projector onto the null space of \mathbf{G} and then each contact force variation $\Delta\lambda_h = \mathbf{P} \Delta\mathbf{q}_r$, produced by modifying joint reference values, satisfies the equation

$$\mathbf{G} \Delta\lambda_h = 0,$$

and then belongs to the internal force subspace.

Summarizing, compliant grasps have been analyzed with a linearized quasi-static model and the main relationships mapping joint references, the controlled inputs, and external disturbances, the wrenches, onto object motions and contact forces have been evaluated in (38.40) and (38.41), respectively.

When applied to grasping, form and force closure have the following interpretations. Assume that a hand grasping an object has its joint angles locked and its palm fixed in space. Then the grasp has *form closure*, or the object is *form-closed*, if it is impossible to move the object, even infinitesimally. Under the same conditions, the grasp has *force closure*, or the object is *force-closed*, if for any non-contact wrench experienced by the object, contact wrench intensities exist that satisfy (38.20) and are consistent with the constraints imposed by the friction models applicable at the contact points. Notice that all form closure grasps are also force closure grasps. When under form closure, the object cannot move even infinitesimally relative to the hand, regardless of the non-contact wrench. Therefore, the hand maintains the object in equilibrium for any external wrench, which is the force closure requirement.

Roughly speaking, form closure occurs when the palm and fingers wrap around the object forming a cage with no *wiggle room* such as the grasp shown in Fig. 38.6. This kind of grasp is also called a *power grasp* [38.32] or *enveloping grasp* [38.33]. However, force closure is possible with fewer contacts, as shown in Fig. 38.7, but in this case, force closure requires the ability to control internal forces. It is also possible for a grasp to have partial form closure, indicating that



Fig. 38.6 The palm and fingers combine to create a very secure form closure grasp of a router

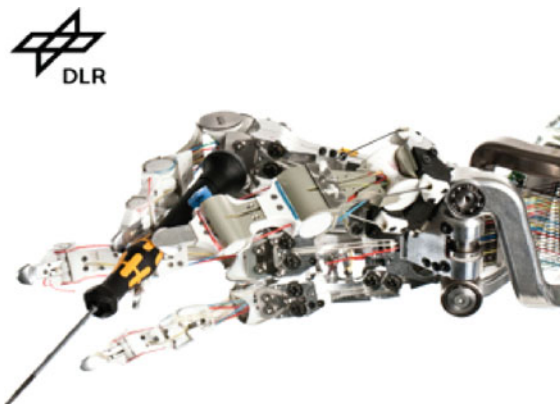


Fig. 38.7 Hand and wrist of the tendon driven DLR Hand Arm System grasping a tool [38.7]. This grasp has a force closure grasp appropriate for dexterous manipulation. (DLR Hand Arm System, Photo courtesy of DLR 2011)

only a subset of the possible degrees of freedom are restrained [38.34]. An example of such a grasp is shown in Fig. 38.8. In this grasp, fingertip placement between the ridges around the periphery of the bottle cap provides form closure against relative rotation about the axis of the helix of the threads and also against translation perpendicular to that axis, but the other three degrees of freedom are restrained through force closure. Strictly speaking, given a grasp of a real object by a human hand it is impossible to prevent relative motion of the object with respect to the palm due to the compliance of the hand and object. Preventing all motion is possible only if the contacting bodies are rigid, as is assumed in most mathematical models employed in grasp analysis.

38.4.1 Form Closure

To make the notion of form closure precise, introduce a signed gap function denoted by $\psi_i(\mathbf{u}, \mathbf{q})$ at each of the n_c contact points between the object and the hand. The gap function is zero at each contact, becomes positive if contact breaks, and negative if penetration occurs. The gap function can be thought of as distance between the contact points. In general, this function is dependent on the shapes of the contacting bodies. Let $\bar{\mathbf{u}}$ and $\bar{\mathbf{q}}$ represent the configurations of the object and hand for a given grasp; then

$$\psi_i(\bar{\mathbf{u}}, \bar{\mathbf{q}}) = 0 \quad \forall i = 1, \dots, n_c. \quad (38.42)$$

The form closure condition can now be stated in terms of a differential change $d\mathbf{u}$ of $\bar{\mathbf{u}}$:

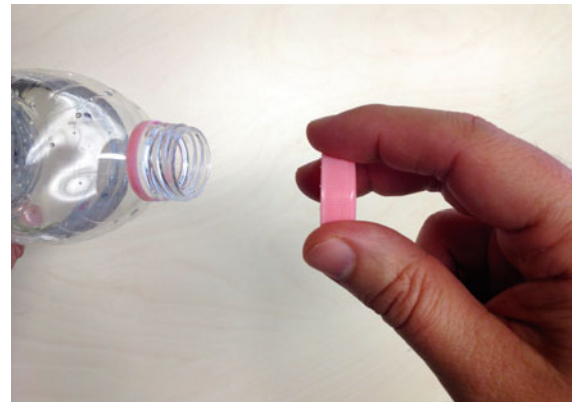


Fig. 38.8 In the grasp depicted, contact with the ridges on the bottle cap create partial form closure in the direction of cap rotation (when screwing it in) and also in the directions of translation perpendicular to the axis of rotation. To achieve complete control over the cap, the grasp achieves force closure over the other three degrees of freedom

Definition 38.6

A grasp $(\bar{\mathbf{u}}, \bar{\mathbf{q}})$ has *form closure* if and only if the following implication holds

$$\boldsymbol{\psi}(\bar{\mathbf{u}} + d\mathbf{u}, \bar{\mathbf{q}}) \geq \mathbf{0} \Rightarrow d\mathbf{u} = \mathbf{0}, \quad (38.43)$$

where $\boldsymbol{\psi}$ is the n_c -dimensional vector of gap functions with i -th component equal to $\psi_i(\mathbf{u}, \mathbf{q})$. By definition, inequalities between vectors imply that the inequality is applied between corresponding components of the vectors.

Expanding the gap function vector in a Taylor series about $\bar{\mathbf{u}}$, yields infinitesimal form closure tests of various orders. Let ${}^\beta \boldsymbol{\psi}(\mathbf{u}, \mathbf{q})$, $\beta = 1, 2, 3, \dots$, denote the Taylor series approximation truncated after the terms of order β in $d\mathbf{u}$. From (38.42), it follows that the first-order approximation is

$${}^1 \boldsymbol{\psi}(\bar{\mathbf{u}} + d\mathbf{u}, \bar{\mathbf{q}}) = \frac{\partial \boldsymbol{\psi}(\mathbf{u}, \mathbf{q})}{\partial \mathbf{u}} \Big|_{(\bar{\mathbf{u}}, \bar{\mathbf{q}})} d\mathbf{u},$$

where $\frac{\partial \boldsymbol{\psi}(\mathbf{u}, \mathbf{q})}{\partial \mathbf{u}} \Big|_{(\bar{\mathbf{u}}, \bar{\mathbf{q}})}$ denotes the partial derivative of $\boldsymbol{\psi}$ with respect to \mathbf{u} evaluated at $(\bar{\mathbf{u}}, \bar{\mathbf{q}})$. Replacing $\boldsymbol{\psi}$ with its approximation of order β in (38.43) implies three relevant cases of order β :

1. If there exists $d\mathbf{u}$ such that ${}^\beta \boldsymbol{\psi}(\bar{\mathbf{u}} + d\mathbf{u}, \bar{\mathbf{q}})$ has at least one strictly positive component, then the grasp does not have form closure of order β .
2. If for every non-zero $d\mathbf{u}$, ${}^\beta \boldsymbol{\psi}(\bar{\mathbf{u}} + d\mathbf{u}, \bar{\mathbf{q}})$ has at least one strictly negative component, then the grasp has form closure of order β .
3. If neither case i) nor case ii) applies for all ${}^\eta \boldsymbol{\psi}(\bar{\mathbf{u}} + d\mathbf{u}, \bar{\mathbf{q}}) \forall \eta \leq \beta$, then higher-order analysis is required to determine the existence of form closure.

Figure 38.9 illustrates form closure concepts using several planar grasps of gray objects by fingers shown as black disks. The concepts are identical for grasps of three-dimensional objects, but are more clearly illustrated in the plane. The grasp on the left has first-order

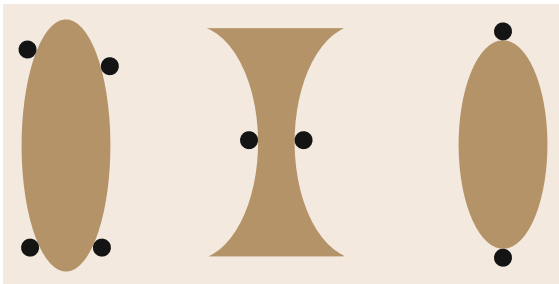


Fig. 38.9 Three planar grasps; two with form closure of different orders and one without form closure

form closure. Note that first-order form closure only involves the first derivatives of the distance functions. This implies that the only relevant geometry in first-order form closure are the locations of the contacts and the directions of the contact normals. The grasp in the center has form closure of higher order, with the specific order depending on the degrees of the curves defining the surfaces of the object and fingers in the neighborhoods of the contacts [38.35]. Second-order form closure analysis depends on the curvatures of the two contacting bodies in addition to the geometric information used to analyze first-order form closure. The grasp on the right does not have form closure of any order, because the object can translate horizontally and rotate about its center.

First-Order Form Closure

First-order form closure exists if and only if the following implication holds

$$\frac{\partial \boldsymbol{\psi}(\mathbf{u}, \mathbf{q})}{\partial \mathbf{u}} \Big|_{(\bar{\mathbf{u}}, \bar{\mathbf{q}})} d\mathbf{u} \geq \mathbf{0} \Rightarrow d\mathbf{u} = \mathbf{0}.$$

The first-order form closure condition can be written in terms of the object twist \mathbf{v}

$$\mathbf{G}_n^T \mathbf{v} \geq \mathbf{0} \Rightarrow \mathbf{v} = \mathbf{0}, \quad (38.44)$$

where $\mathbf{G}_n^T = \partial \boldsymbol{\psi} / \partial \mathbf{u} \mathbf{V} \in \mathbb{R}^{n_c \times 6}$. Recall that \mathbf{V} is the kinematic map defined in (38.1). Also notice that \mathbf{G}_n is the grasp matrix, when all contact points are frictionless.

Because the gap functions only quantify distances, the product $\mathbf{G}_n^T \mathbf{v}$ is the vector of normal components of the instantaneous velocities of the object at the contact points (which must be non-negative to prevent interpenetration). This in turn implies that the grasp matrix is the one that would result from the assumption that all contacts are of the type PwoF.

An equivalent condition in terms of the contact wrench intensity vector $\boldsymbol{\lambda}_n \in \mathbb{R}^{n_c}$ can be stated as follows. A grasp has first-order form closure if and only if

$$\left. \begin{array}{l} \mathbf{G}_n \boldsymbol{\lambda}_n = -\mathbf{g} \\ \boldsymbol{\lambda}_n \geq \mathbf{0} \end{array} \right\} \forall \mathbf{g} \in \mathbb{R}^6. \quad (38.45)$$

The physical interpretation of this condition is that equilibrium can be maintained under the assumption that the contacts are frictionless. Note that the components of $\boldsymbol{\lambda}_n$ are the magnitudes of the normal components of the contact forces. The subscript $(\cdot)_n$ is used to emphasize that $\boldsymbol{\lambda}_n$ contains no other force or moment components.

Since \mathbf{g} must be in the range of \mathbf{G}_n for equilibrium to be satisfied, and since \mathbf{g} is an arbitrary element of \mathbb{R}^6 , then in order for condition (38.45) to be satisfied, the rank of \mathbf{G}_n must be six. Assuming $\text{rank}(\mathbf{G}_n) = 6$, another equivalent mathematical statement of first-order form closure is: there exists $\boldsymbol{\lambda}_n$ such that the following two conditions hold [38.36]

$$\begin{aligned} \mathbf{G}_n \boldsymbol{\lambda}_n &= \mathbf{0}, \\ \boldsymbol{\lambda}_n &> \mathbf{0}. \end{aligned} \tag{38.46}$$

This means that there exists a set of strictly compressive normal contact forces in the null space of \mathbf{G}_n . In other words, one can squeeze the object as tightly as desired while maintaining equilibrium. A second interpretation of this condition is that the non-negative span of the columns of \mathbf{G}_n must equal \mathbb{R}^6 . Equivalently, the convex hull of the columns of \mathbf{G}_n must strictly contain the origin of \mathbb{R}^6 . As will be seen, the span and hull interpretations will provide a conceptual link called *frictional form closure* that lies between form closure and force closure.

The duality of conditions (38.44) and (38.45) can be seen clearly by examining the set of wrenches that can be applied by frictionless contacts and the corresponding set of possible object twists. For this discussion, it is useful to give definitions of cones and their duals.

Definition 38.7

A cone C is a set of vectors $\boldsymbol{\zeta}$ such that for every $\boldsymbol{\zeta}$ in C , every non-negative scalar multiple of $\boldsymbol{\zeta}$ is also in C .

Equivalently, a cone is a set of vectors closed under addition and non-negative scalar multiplication.

Definition 38.8

Given a cone C with elements $\boldsymbol{\zeta}$, the dual cone C^* with elements $\boldsymbol{\zeta}^*$, is the set of vectors such that the dot product of $\boldsymbol{\zeta}^*$ with each vector in C is non-negative. Mathematically

$$C^* = \{ \boldsymbol{\zeta}^* \mid \boldsymbol{\zeta}^T \boldsymbol{\zeta}^* \geq 0, \forall \boldsymbol{\zeta} \in C \}. \tag{38.47}$$

See Example 4.

First-Order Form Closure Requirements

Several useful necessary conditions for form closure are known. In 1897 *Somov* proved that at least seven contacts are necessary to form close a rigid object with six degrees of freedom [38.37, 38]. *Lakshminarayana* generalized this to prove that $n_v + 1$ contacts are necessary to form close an object with n_v degrees

of freedom [38.34] (based on *Goldman and Tucker* 1956 [38.39]) (Table 38.9). This led to the definition of partial form closure that was mentioned above in the discussion of the hand grasping the bottle cap. *Markenscoff* and *Papadimitriou* determined a tight upper bound, showing that for all objects whose surfaces are not surfaces of revolution, at most $n_v + 1$ contacts are necessary [38.40]. Form closure is impossible to achieve for surfaces of revolution.

To emphasize the fact that $n_v + 1$ contacts are necessary and *not* sufficient, consider grasping a cube with seven or more points of contact. If all contacts are on one face, then clearly, the grasp does not have form closure.

First-Order Form Closure Tests

Because form closure grasps are very secure, it is desirable to design or synthesize such grasps. To do this, one needs a way to test candidate grasps for form closure, and rank them, so that the *best* grasp can be chosen. One reasonable measure of form closure can be derived from the geometric interpretation of the condition (38.46). The null space constraint and the positivity of $\boldsymbol{\lambda}_n$ represent the addition of the columns of \mathbf{G}_n scaled by the components of $\boldsymbol{\lambda}_n$. Any choice of $\boldsymbol{\lambda}_n$ closing this loop is in $\mathcal{N}(\mathbf{G}_n)$. For a given loop, if the magnitude of the smallest component of $\boldsymbol{\lambda}_n$ is positive, then the grasp has form closure, otherwise it does not. Let us denote this smallest component by d . Since such a loop, and hence d , can be scaled arbitrarily, $\boldsymbol{\lambda}_n$ must be bounded.

After verifying that \mathbf{G}_n has full row rank, a quantitative form closure test based on the above observations can be formulated as a linear program (LP) in the unknowns d and $\boldsymbol{\lambda}_n$ as follows

$$\text{LP1: maximize: } d \tag{38.48}$$

$$\text{subject to: } \mathbf{G}_n \boldsymbol{\lambda}_n = \mathbf{0} \tag{38.49}$$

$$\mathbf{I} \boldsymbol{\lambda}_n - \mathbf{1}d \geq \mathbf{0} \tag{38.50}$$

$$d \geq 0 \tag{38.51}$$

$$\mathbf{1}^T \boldsymbol{\lambda}_n \leq n_c, \tag{38.52}$$

where $\mathbf{I} \in \mathbb{R}^{n_c \times n_c}$ is the identity matrix and $\mathbf{1} \in \mathbb{R}^{n_c}$ is a vector with all components equal to 1. The last inequality is designed to prevent this LP from becoming unbounded. A typical LP solution algorithm determines

Table 38.9 Minimum number of contacts n_c required to form close an object with n_v degrees of freedom

n_v	n_c
3 (planar grasp)	4
6 (spatial grasp)	7
n_v (general)	$n_v + 1$

infeasibility or unboundedness of the constraints in Phase I of the algorithm, and considers the result before attempting to calculate an optimal value [38.41]. If LP1 is infeasible, or if the optimal value d^* is zero, then the grasp is not form closed.

The quantitative form closure test (38.48)–(38.52) has $n_c + 8$ constraints and $n_c + 1$ unknowns. For a typical grasp with $n_c < 10$, this is a small linear program that can be solved very quickly using the simplex method. However, one should note that d^* is dependent on the choice of units used when forming \mathbf{G}_n . It would be advisable to non-dimensionalize the components of the wrenches to avoid dependence of the optimal d on one's choice of units. This could be done by dividing the first three rows of \mathbf{G}_n by a characteristic force and the last three rows by a characteristic moment. If one desires a binary test, LP1 can be converted into one by dropping the last constraint (38.52) and applying only Phase I of the simplex algorithm.

In summary, quantitative form closure testing is a two-step process:

Form Closure Test.

1. Compute $\text{rank}(\mathbf{G}_n)$.
 - a) If $\text{rank}(\mathbf{G}_n) \neq n_v$, then form closure does not exist. Stop.
 - b) If $\text{rank}(\mathbf{G}_n) = n_v$, continue.
2. Solve LP1.
 - a) If $d^* = 0$, then form closure does not exist.
 - b) If $d^* > 0$, then form closure exists and $d^* n_c$ is a crude measure of how far the grasp is from losing form closure.

See Example 5, Part 1.

Variations of the Test. If the rank test fails, then the grasp could have partial form closure over as many as $\text{rank}(\mathbf{G}_n)$ degrees of freedom. If one desires to test this, then LP1 must be solved using a new \mathbf{G}_n formed by retaining only the rows corresponding to the degrees of freedom for which partial form closure is to be tested. If $d^* > 0$, then partial form closure exists.

A second variation arises when one knows in advance that the object is already partially constrained. For example, in the case of a steering wheel, the driver knows, that relative to her, the steering wheel has only one degree of freedom. A form closure grasp suitable for driving would be required only to restraint the wheel's rotation about the steering column. In general, assume that the object is constrained by a set of bilateral constraints, which can be written as

$$\mathbf{B}^T \mathbf{v} = \mathbf{0}. \quad (38.53)$$

With these additional constraints, the form closure property can be expressed as follows

$$\left. \begin{array}{l} \mathbf{G}_n^T \mathbf{v} \geq \mathbf{0} \\ \mathbf{B}^T \mathbf{v} = \mathbf{0} \end{array} \right\} \Rightarrow \mathbf{v} = \mathbf{0}, \quad (38.54)$$

which can be shown to be equivalent to

$$\overline{\mathbf{G}}_n^T \boldsymbol{\rho} \geq \mathbf{0} \Rightarrow \boldsymbol{\rho} = \mathbf{0}, \quad (38.55)$$

where $\boldsymbol{\rho}$ is an arbitrary vector with length equal to the dimension of the null space of \mathbf{B}^T and $\overline{\mathbf{G}}_n = \mathbf{A}_B \mathbf{G}_n$, where \mathbf{A}_B is an annihilator of the column space of \mathbf{B} . One possible way to construct this annihilator is $\mathbf{A}_B = (\mathbf{N}(\mathbf{B}^T))^T$, where $\mathbf{N}(\mathbf{B}^T)$ is a matrix whose columns form a basis for the null space of \mathbf{B}^T . Also note that $\mathbf{N}(\mathbf{B}^T)\boldsymbol{\rho}$ is a possible twist of the object consistent with the bilateral constraints (i.e., the twists that must be eliminated by the unilateral constraints).

The form closure condition for an object partially constrained by bilateral constraints can also be stated in terms of wrenches

$$\left. \begin{array}{l} \overline{\mathbf{G}}_n \boldsymbol{\lambda}_n = \mathbf{0}, \\ \boldsymbol{\lambda}_n > \mathbf{0}. \end{array} \right\} \quad (38.56)$$

Notice that twist conditions (38.44) and (38.55) and wrench conditions (38.46) and (38.56) are formally analogous, and therefore, the quantitative form closure test can be applied by substituting $\overline{\mathbf{G}}_n$ for \mathbf{G}_n and $(n_v - \text{rank}(\mathbf{B}))$ for n_v . For detailed information on the derivations of the constrained form closure conditions, please refer to [38.42].

See Example 5, Part 2.

Monotonicity. In grasp synthesis, sometimes it is desirable for the grasp metric to increase monotonically with the number of contact points, the intuition being, that adding contacts to a stable grasp will make it more stable. The solution d^* does not have this property. However `formClosure.m`, a Matlab function which is available at [38.43], returns $d^* n_c$ as the metric, because it nearly maintains monotonicity when adding random contacts to random grasps. This can be demonstrated by running `test_monotonicity.m`.

One can design metrics that are monotonic with norms on the set of wrenches that the hand can apply. Let the polytope $\mathcal{G} = \{\mathbf{g} | \mathbf{g} = \mathbf{G}_n \boldsymbol{\lambda}_n, \mathbf{0} \leq \boldsymbol{\lambda}_n \leq \mathbf{1}\}$ denote the wrench space, which is the set of wrenches that can be applied by the hand if the contact forces magnitudes are limited to one. A metric proposed by Ferrari and Canny [38.44] is the radius of the largest sphere in \mathcal{G} with origin at the origin of the wrench space. The radius is greater than 0 if and only if the grasp has form

closure. In addition, adding a contact point will always produce a new \mathcal{G} that is a superset of the original \mathcal{G} . Thus the radius of the sphere cannot reduce as a result. Hence the monotonicity property holds.

See Example 5, Part 3.

Planar Simplifications

In the planar case, *Nguyen* [38.45] developed a graphical qualitative test for form closure. Figure 38.10 shows a form closure grasp with four contacts. To test form closure one partitions the normals into two groups of two. Let C_1 be the non-negative span of two normals in one pair and C_2 be the non-negative span of the other pair. A grasp has form closure if and only if C_1 and C_2 or $-C_1$ and $-C_2$ see each other for any pairings. Two cones see each other if the open line segment defined by the vertices of the cones lies in the interior of both cones. In the presence of more than four contacts, if any set of four contacts satisfies this condition, then the grasp has form closure.

Notice that this graphical test can be difficult to execute for grasps with more than four contacts. Also, it does not extend to grasps of three-dimensional (3-D) objects and does not provide a closure measure.

38.4.2 Force Closure

A grasp has force closure, or is force-closed, if the grasp can be maintained in the face of any object wrench. Force closure is similar to form closure, but relaxed to allow friction forces to help balance the object wrench. A benefit of including friction in the analysis is the reduction in the number of contact points needed for closure. A three-dimensional object with six degrees of freedom requires seven contacts for form closure, but for force closure, only two contacts are needed if they are modeled as soft fingers, and only three (non-collinear) contacts are needed if they are modeled as hard fingers.

Force closure relies on the ability of the hand to squeeze arbitrarily tightly in order to compensate for large applied wrenches that can only be resisted by friction. Figure 38.15 shows a grasped polygon. Con-

sider applying a wrench to the object that is a pure force acting upward along the y -axis of the inertial frame. It seems intuitive that if there is enough friction, the hand will be able to squeeze the object with friction forces preventing the object's upward escape. Also, as the applied force increases in magnitude, the magnitude of the squeezing force will have to increase accordingly.

Since force closure is dependent on the friction models, common models will be introduced before giving formal definitions of force closure.

Friction Models

Recall the components of force and moment transmitted through contact i under the various contact models given earlier in Table 38.4. At contact point i , the friction law imposes constraints on the components of the contact force and moment. Specifically, the frictional components of λ_i are constrained to lie inside a limit surface, denoted by \mathcal{L}_i , that scales linearly with the product $\mu_i f_{in}$, where μ_i is the coefficient of friction at contact i . In the case of Coulomb friction, the limit surface is a circle of radius $\mu_i f_{in}$. The Coulomb friction cone \mathcal{F}_i is a subset of \mathbb{R}^3

$$\mathcal{F}_i = \{(f_{in}, f_{it}, f_{io}) \mid \sqrt{f_{it}^2 + f_{io}^2} \leq \mu_i f_{in}\}. \quad (38.57)$$

More generally, the friction laws of interest have limit surfaces defined in the space of friction components, $\mathbb{R}^{n\lambda_i-1}$ and friction cones \mathcal{F}_i defined in the space of λ_i , $\mathbb{R}^{n\lambda_i}$. They can be written as follows

$$\mathcal{F}_i = \{\lambda_i \in \mathbb{R}^{n\lambda_i} \mid \|\lambda_i\|_w \leq f_{in}\}, \quad (38.58)$$

where $\|\lambda_i\|_w$ denotes a weighted quadratic norm of the friction components at contact i . The limit surface is defined by $\|\lambda_i\|_w = f_{in}$.

Table 38.10 defines useful weighted quadratic norms for the three contact models: PwoF, HF, and SF. The parameter μ_i is the friction coefficient for the tangential forces, ν_i is the torsional friction coefficient, and a is the characteristic length of the object that is used to ensure consistent units for the norm of the SF model.

Table 38.10 Norms for the three main contact models

Model	$\ \lambda_i\ _w$
PwoF	0
HF	$\frac{1}{\mu_i} \sqrt{f_{it}^2 + f_{io}^2}$
SF	$\frac{1}{\mu_i} \sqrt{f_{it}^2 + f_{io}^2} + \frac{1}{a\nu_i} m_{in} $

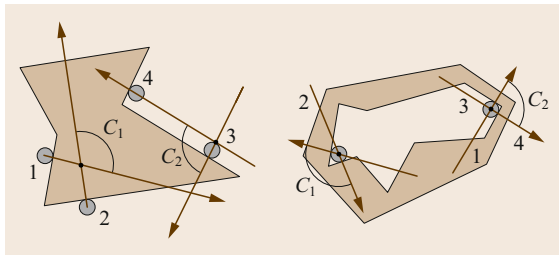


Fig. 38.10 Planar grasps with first-order form closure

Remark 38.4

There are several noteworthy points to be made about the friction cones. First, all of them implicitly or explicitly constrain the normal component of the contact force to be non-negative. The cone for SF contacts has a cylindrical limit surface with circular cross section in the (f_{it}, f_{io}) -plane and rectangular cross section in the (f_{it}, m_{in}) -plane. With this model, the amount of torsional friction that can be transmitted is independent of the lateral friction load. An improved model that couples the torsional friction limit with the tangential limit was studied by Howe and Cutkosky [38.46].

A Force Closure Definition

One common definition of force closure can be stated simply by modifying condition (38.45) to allow each contact force to lie in its friction cone rather than along the contact normal. Because this definition does not consider the hand's ability to control contact forces, this definition will be referred to as *frictional form closure*. A grasp will be said to have frictional form closure if and only if the following condition is satisfied

$$\begin{cases} \mathbf{G}\boldsymbol{\lambda} = -\mathbf{g} \\ \boldsymbol{\lambda} \in \mathcal{F} \end{cases} \forall \mathbf{g} \in \mathbb{R}^{n_v},$$

where \mathcal{F} is the composite friction cone defined as:

$$\begin{aligned} \mathcal{F} &= \mathcal{F}_1 \times \cdots \times \mathcal{F}_{n_c} \\ &= \{\boldsymbol{\lambda} \in \mathbb{R}^m \mid \lambda_i \in \mathcal{F}_i; i = 1, \dots, n_c\}, \end{aligned}$$

and each \mathcal{F}_i is defined by (38.58) and one of the models listed in Table 38.10.

Letting $\text{Int}(\mathcal{F})$ denote the interior of the composite friction cone, Murray et al. give the following equivalent definition [38.19]:

Definition 38.9

(Proposition 5.2, Murray et al.) A grasp has *frictional form closure* if and only if the following conditions are satisfied:

1. $\text{rank}(\mathbf{G}) = n_v$
2. $\exists \boldsymbol{\lambda}$ such that $\mathbf{G}\boldsymbol{\lambda} = \mathbf{0}$ and $\boldsymbol{\lambda} \in \text{Int}(\mathcal{F})$.

These conditions define what Murray et al. call *force closure*. The force closure definition adopted here is stricter than frictional form closure; it additionally requires that the hand be able to control the internal object forces.

Definition 38.10

A grasp has *force closure* if and only if

$$\text{rank}(\mathbf{G}) = n_v, \mathcal{N}(\mathbf{G}) \cap \mathcal{N}(\mathbf{J}^T) = \mathbf{0},$$

and there exists $\boldsymbol{\lambda}$ such that $\mathbf{G}\boldsymbol{\lambda} = \mathbf{0}$ and $\boldsymbol{\lambda} \in \text{Int}(\mathcal{F})$.

The full row rank condition on the matrix \mathbf{G} is the same condition required for form closure, although \mathbf{G} is different from \mathbf{G}_n used to determine form closure. If the rank test passes, then one must still find $\boldsymbol{\lambda}$ satisfying the remaining three conditions. Of these, the null space intersection test can be performed easily by linear programming techniques, but the friction cone constraint is quadratic, and thus forces one to use non-linear programming techniques. While exact non-linear tests have been developed [38.47], only approximate tests will be presented here.

Approximate Force Closure Tests

Any of the friction cones discussed can be approximated as the non-negative span of a finite number n_g of generators s_{ij} of the friction cone. Given this, one can represent the set of applicable contact wrenches at contact i as follows

$$\mathbf{G}_i \boldsymbol{\lambda}_i = \mathbf{S}_i \boldsymbol{\sigma}_i, \quad \boldsymbol{\sigma}_i \geq 0,$$

where $\mathbf{S}_i = [s_{i1} \cdots s_{in_g}]$ and $\boldsymbol{\sigma}_i$ is a vector of non-negative generator weights. If contact i is frictionless, then $n_g = 1$ and $\mathbf{S}_i = [\hat{\mathbf{n}}_i^T ((\mathbf{c}_i - \mathbf{p}) \times \hat{\mathbf{n}}_i)^T]^T$.

If contact i is of type HF, we represent the friction cone by the non-negative sum of uniformly spaced contact force generators (Fig. 38.11) whose non-negative span approximates the Coulomb cone with an inscribed regular polyhedral cone. This leads to the following def-

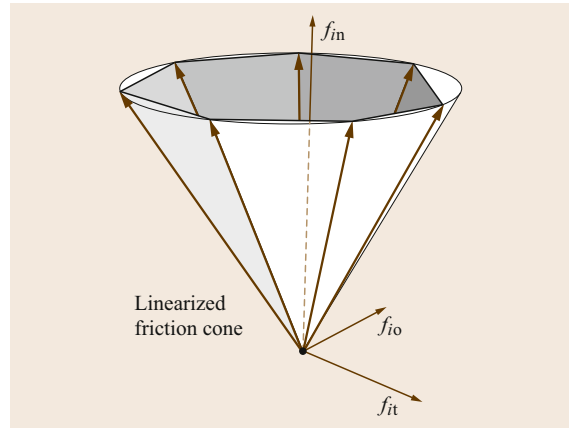


Fig. 38.11 Quadratic cone approximated as a polyhedral cone with seven generators

inition of \mathbf{S}_i

$$\mathbf{S}_i = \begin{pmatrix} \cdots & 1 & \cdots \\ \cdots & \mu_i \cos(2k\pi/n_g) & \cdots \\ \cdots & \mu_i \sin(2k\pi/n_g) & \cdots \end{pmatrix}, \quad (38.59)$$

where the index k varies from one to n_g . If one prefers to approximate the quadratic friction cone by a circumscribing polyhedral cone, one simply replaces μ_i in the above definition with $\mu_i / \cos(\pi/n_g)$.

The adjustment needed for the SF model is quite simple. Since the torsional friction in this model is decoupled from the tangential friction, its generators are given by $[1 \ 0 \ 0 \ \pm bv_i]^T$. Thus \mathbf{S}_i for the SF model is

$$\mathbf{S}_i = \left(\begin{array}{ccc|cc} \cdots & 1 & \cdots & 1 & 1 \\ \cdots & \mu_i \cos(2k\pi/n_g) & \cdots & 0 & 0 \\ \cdots & \mu_i \sin(2k\pi/n_g) & \cdots & 0 & 0 \\ \cdots & 0 & \cdots & bv_i & -bv_i \end{array} \right), \quad (38.60)$$

where b is the characteristic length used to unify units. The set of total contact wrenches that may be applied by the hand without violating the contact friction law at any contact can be written as

$$\mathbf{G}\boldsymbol{\lambda} = \mathbf{S}\boldsymbol{\sigma}, \quad \boldsymbol{\sigma} \geq \mathbf{0},$$

where

$$\mathbf{S} = (\mathbf{S}_1, \dots, \mathbf{S}_{n_g})$$

and

$$\boldsymbol{\sigma} = (\boldsymbol{\sigma}_1^T \cdots \boldsymbol{\sigma}_{n_g}^T)^T.$$

It is convenient to reformulate the friction constraints in a dual form

$$\mathbf{F}_i \boldsymbol{\lambda}_i \geq \mathbf{0}. \quad (38.61)$$

In this form, each row of \mathbf{F}_i is normal to a face formed by two adjacent generators of the approximate cone. For an HF contact, row i of \mathbf{F}_i can be computed as the cross product of \mathbf{s}_i and \mathbf{s}_{i+1} . In the case of an SF contact, the generators are of dimension four, so simple cross products will not suffice. However, general methods exist to perform the conversion from the generator form to the face normal form [38.39].

The face normal constraints for all contacts can be combined into the following compact form

$$\mathbf{F}\boldsymbol{\lambda} \geq \mathbf{0}, \quad (38.62)$$

where $\mathbf{F} = \text{Blockdiag}(\mathbf{F}_1, \dots, \mathbf{F}_{n_c})$.

Let $\mathbf{e}_i \in \mathbb{R}^{n_{\lambda i}}$ be the first row of \mathbf{H}_i . Further let

$$\mathbf{e} = [\mathbf{e}_1, \dots, \mathbf{e}_{n_c}] \in \mathbb{R}^{n_{\lambda}}$$

and let

$$\mathbf{E} = \text{Blockdiag}(\mathbf{e}_1, \dots, \mathbf{e}_{n_c}) \in \mathbb{R}^{n_{\lambda} \times n_c}.$$

The following linear program is a quantitative test for frictional form closure. The optimal objective function value d^* is a measure of the distance the contact forces are from the boundaries of their friction cones, and hence a crude measure of how far a grasp is from losing frictional form closure.

$$\begin{array}{ll} \text{LP2:} & \text{maximize:} & d \\ & \text{subject to:} & \mathbf{G}\boldsymbol{\lambda} = \mathbf{0} \\ & & \mathbf{F}\boldsymbol{\lambda} - \mathbf{1}d \geq \mathbf{0} \\ & & d \geq 0 \\ & & \mathbf{e}\boldsymbol{\lambda} \leq n_c. \end{array}$$

The last inequality in LP2 is simply the sum of the magnitudes of the normal components of the contact forces. After solving LP2, if $d^* = 0$ frictional form closure does not exist, but if $d^* > 0$, then it does.

If the grasp has frictional form closure, the last step to determine the existence of force closure is to verify the condition $\mathcal{N}(\mathbf{G}) \cap \mathcal{N}(\mathbf{J}^T) = \mathbf{0}$. If it holds, then the grasp has force closure. This condition is easy to verify with another linear program LP3.

$$\begin{array}{ll} \text{LP3:} & \text{maximize:} & d \\ & \text{subject to:} & \mathbf{G}\boldsymbol{\lambda} = \mathbf{0} \\ & & \mathbf{J}^T \boldsymbol{\lambda} = \mathbf{0} \\ & & \mathbf{E}\boldsymbol{\lambda} - \mathbf{1}d \geq \mathbf{0} \\ & & d \geq 0 \\ & & \mathbf{e}\boldsymbol{\lambda} \leq n_c. \end{array}$$

In summary, force closure testing is a three-step process.

Approximate Force Closure Test.

1. Compute $\text{rank}(\mathbf{G})$.
 - a) If $\text{rank}(\mathbf{G}) \neq n_v$, then force closure does not exist. Stop.
 - b) If $\text{rank}(\mathbf{G}) = n_v$, continue.
2. Solve LP2: *Test frictional form closure*.
 - a) If $d^* = 0$, then frictional form closure does not exist. Stop.
 - b) If $d^* > 0$, then frictional form closure exists and d^* is a crude measure of how far the grasp is from losing frictional form closure.

3. Solve LP3: *Test control of internal force.*
- If $d^* > 0$, then force closure does not exist.
 - If $d^* = 0$, then force closure exists.

Variation of the Test. A variation of the approximate force closure test arises when the object is partially constrained with the bilateral constraints described by (38.53), in such a cases the definitions of frictional form closure becomes

$$\begin{aligned} \bar{\mathbf{G}}\boldsymbol{\lambda} &= \mathbf{0}, \\ \boldsymbol{\lambda} &\in \text{int}(\mathcal{F}), \end{aligned} \quad (38.63)$$

where $\bar{\mathbf{G}} = \mathbf{A}_B \mathbf{G}$, \mathbf{A}_B is an annihilator of the column space of \mathbf{B} . Similarly, the force closure condition can be stated as

$$\begin{aligned} \bar{\mathbf{G}}\boldsymbol{\lambda} &= \mathbf{0}, \\ \boldsymbol{\lambda} &\in \text{int}(\mathcal{F}), \\ \mathcal{N}(\bar{\mathbf{G}}) \cap \mathcal{N}(\mathbf{J}^T) &= \mathbf{0}, \end{aligned} \quad (38.64)$$

Since the frictional form closure definition (38.63) is analogous to Definition 38.9 and the force closure definition (38.64) is analogous to Definition 38.10, the force closure test can be applied by substituting $\bar{\mathbf{G}}$ for

38.5 Examples

38.5.1 Example 1: Grasped Sphere

Part 1: $\tilde{\mathbf{G}}$ and $\tilde{\mathbf{J}}$

Figure 38.12 shows a planar projection of a three-dimensional sphere of radius r grasped by two fingers, which make two contacts at angles θ_1 and θ_2 . The frames $\{\mathbf{C}\}_1$ and $\{\mathbf{C}\}_2$ are oriented so that their $\hat{\mathbf{d}}$ -directions point out of the plane of the figure (as indicated by the small filled circles at the contact points). The axes of the frames $\{\mathbf{N}\}$ and $\{\mathbf{B}\}$ were chosen to be axis-aligned with coincident origins located at the center of the sphere. The z -axes are pointing out of the page. Observe that since the two joint axes of the left finger are perpendicular to the (x, y) -plane, it operates in that plane for all time. The other finger has three revolute joints. Because its first and second axes, $\hat{\mathbf{z}}_3$ and $\hat{\mathbf{z}}_4$, currently lie in the plane, rotation about $\hat{\mathbf{z}}_3$ will cause $\hat{\mathbf{z}}_4$ to attain an out-of-plane component and would cause the finger tip at contact 2 to leave the plane.

In the current configuration, the rotation matrix for the i -th contact frame is defined as follows

$$\mathbf{R}_i = \begin{pmatrix} -\cos(\theta_i) & \sin(\theta_i) & 0 \\ -\sin(\theta_i) & -\cos(\theta_i) & 0 \\ 0 & 0 & 1 \end{pmatrix}. \quad (38.66)$$

\mathbf{G} , provided that, $(n_\nu - \text{rank}(\mathbf{B}))$ is substituted for n_ν . For detailed information on the derivation of these conditions, please refer to [38.42].

See Example 1, Part 6.

Planar Simplifications

In planar grasping systems, the approximate method described above is exact. This is because the SF models are meaningless, since rotations about the contact normal would cause motions out of the plane. With regard to the HF model, for planar problems, the quadratic friction cone becomes linear, with its cone represented exactly as

$$\mathbf{F}_i = \frac{1}{\sqrt{1 + \mu_i^2}} \begin{pmatrix} \mu_i & 1 \\ \mu_i & -1 \end{pmatrix}. \quad (38.65)$$

Nguyen's graphical form closure test can be applied to planar grasps with two frictional contacts [38.45]. The only change is that the four contact normals are replaced by the four generators of the two friction cones. However, the test can only determine frictional form closure, since it does not incorporate the additional information needed to determine force closure.

The vector from the origin of $\{\mathbf{N}\}$ to the i -th contact point is given by

$$\mathbf{c}_i - \mathbf{p} = r \begin{pmatrix} \cos(\theta_i) & \sin(\theta_i) & 0 \end{pmatrix}^T. \quad (38.67)$$

Substituting into (38.3) and (38.6) yields the complete grasp matrix for contact i

$$\tilde{\mathbf{G}}_i = \left(\begin{array}{ccc|ccc} -c_i & s_i & 0 & & & \\ -s_i & -c_i & 0 & & & \\ 0 & 0 & 1 & & & \\ \hline 0 & 0 & rs_i & -c_i & s_i & 0 \\ 0 & 0 & -rc_i & -s_i & -c_i & 0 \\ 0 & -r & 0 & 0 & 0 & 1 \end{array} \right), \quad (38.68)$$

where $\mathbf{0} \in \mathbb{R}^{3 \times 3}$ is the zero matrix and c_i and s_i are abbreviations for $\cos(\theta_i)$ and $\sin(\theta_i)$, respectively. The complete grasp matrix is defined as: $\tilde{\mathbf{G}} = (\tilde{\mathbf{G}}_1 \tilde{\mathbf{G}}_2) \in \mathbb{R}^{6 \times 12}$.

The accuracy of this matrix can be verified by inspection, according to Remark 38.2. For example, the first column is the unit wrench of the unit contact normal; the first three components are the direction cosines

of \hat{n}_i and the last three are $(c_i - p) \times \hat{n}_i$. Since \hat{n}_i is collinear with $(c_i - p)$, the cross products (the last three components of the column) are zero. The last three components of the second column represent the moment of \hat{t}_i about the x -, y -, and z -axes of $\{N\}$. Since \hat{t}_i lies in the (x, y) -plane, the moments with the x - and y -axes are zero. Clearly \hat{t}_i produces a moment of $-r$ about the z -axis.

Construction of the hand Jacobian \tilde{J}_i for contact i requires knowledge of the joint axis directions and the origins of the frames fixed to the links of each finger. Figure 38.13 shows the hand in the same configuration as in Fig. 38.12, but with some additional data needed to construct the hand Jacobian. Assume that the origins of the joint frames lie in the plane of the figure. In the current configuration, the quantities of interest for contact 1, expressed in $\{C\}_1$ are

$$c_1 - \zeta_1 = (l_2 \quad l_1 \quad 0)^T, \tag{38.69}$$

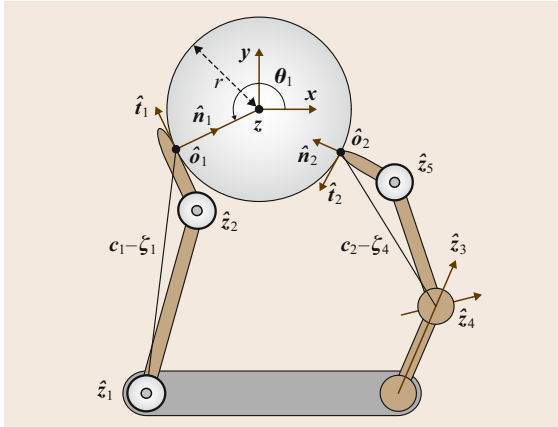


Fig. 38.12 A sphere grasped by a two-fingered hand with 5 revolute joints

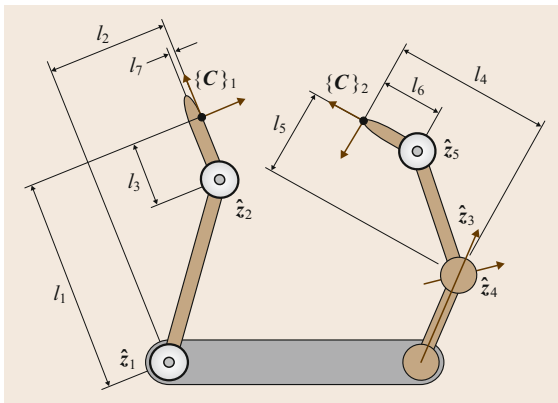


Fig. 38.13 Relevant data for the hand Jacobian in Fig. 38.12

$$c_1 - \zeta_2 = (l_7 \quad l_3 \quad 0)^T, \tag{38.70}$$

$$\hat{z}_1 = \hat{z}_2 = (0 \quad 0 \quad 1)^T. \tag{38.71}$$

The quantities of interest for contact 2, in $\{C\}_2$ are

$$c_2 - \zeta_3 = c_2 - \zeta_4 = (l_4 \quad l_5 \quad 0)^T, \tag{38.72}$$

$$c_2 - \zeta_5 = (l_6 \quad 0 \quad 0)^T, \tag{38.73}$$

$$\hat{z}_3 = (0 \quad 1 \quad 0)^T, \tag{38.74}$$

$$\hat{z}_4(q_3) = \frac{\sqrt{2}}{2} (-1 \quad 1 \quad 0)^T, \tag{38.75}$$

$$\hat{z}_5(q_3, q_4) = (0 \quad 0 \quad 1)^T. \tag{38.76}$$

Generally all of the components of the $c - \zeta$ and \hat{z} vectors (including the components that are zero in the current configuration), are functions of q and u . The dependencies of the \hat{z} vectors are shown explicitly.

Substituting into (38.14)₂, (38.11) and (38.8) yields the complete hand Jacobian $\tilde{J} \in \mathbb{R}^{12 \times 5}$

$$\tilde{J} = \left(\begin{array}{cc|ccc} -l_1 & -l_3 & & & \\ l_2 & l_7 & & & \\ 0 & 0 & & & \\ 0 & 0 & & \mathbf{0} & \\ 0 & 0 & & & \\ 1 & 1 & & & \\ \hline & & 0 & 0 & 0 \\ & & 0 & 0 & l_6 \\ & & l_4 & \frac{\sqrt{2}}{2}(l_4 + l_5) & 0 \\ \mathbf{0} & & 0 & -\frac{\sqrt{2}}{2} & 0 \\ & & -1 & -\frac{\sqrt{2}}{2} & 0 \\ & & 0 & 0 & 1 \end{array} \right).$$

The horizontal dividing line partitions \tilde{J} into \tilde{J}_1 (on top) and \tilde{J}_2 (on the bottom). The columns correspond to joints 1 through 5. The block diagonal structure is a result of the fact that finger i directly affects only contact i .

Example 1, Part 2: **G** and **J**

Assume that the contacts in Fig. 38.12 are both of type SF. Then the selection matrix **H** is given by

$$\mathbf{H} = \left(\begin{array}{cccccc|cccc} 1 & 0 & 0 & 0 & 0 & 0 & & & & \\ 0 & 1 & 0 & 0 & 0 & 0 & & & & \mathbf{0} \\ 0 & 0 & 1 & 0 & 0 & 0 & & & & \\ 0 & 0 & 0 & 1 & 0 & 0 & & & & \\ \hline & & & & & & 1 & 0 & 0 & 0 & 0 & 0 \\ & & & & & & 0 & 1 & 0 & 0 & 0 & 0 \\ \mathbf{0} & & & & & & 0 & 0 & 1 & 0 & 0 & 0 \\ & & & & & & 0 & 0 & 0 & 1 & 0 & 0 \end{array} \right),$$

thus the matrices $\mathbf{G}^T \in \mathbb{R}^{8 \times 6}$ and $\mathbf{J} \in \mathbb{R}^{8 \times 5}$ are constructed by removing rows 5, 6, 11, and 12 from $\tilde{\mathbf{G}}^T$ and $\tilde{\mathbf{J}}$

$$\mathbf{G}^T = \begin{pmatrix} -c_1 & -s_1 & 0 & 0 & 0 & 0 \\ s_1 & -c_1 & 0 & 0 & 0 & -r \\ 0 & 0 & 1 & r s_1 & -r c_1 & 0 \\ 0 & 0 & 0 & -c_1 & -s_1 & 0 \\ -c_2 & -s_2 & 0 & 0 & 0 & 0 \\ s_2 & -c_2 & 0 & 0 & 0 & -r \\ 0 & 0 & 1 & r s_2 & -r c_2 & 0 \\ 0 & 0 & 0 & -c_2 & -s_2 & 0 \end{pmatrix}, \quad (38.77)$$

$$\mathbf{J} = \begin{pmatrix} -l_1 & -l_3 & & & \\ l_2 & l_7 & & & \mathbf{0} \\ 0 & 0 & & & \\ 0 & 0 & & & \\ \mathbf{0} & & 0 & 0 & 0 \\ & & 0 & 0 & l_6 \\ & & l_4 & \frac{\sqrt{2}}{2}(l_4 + l_5) & 0 \\ & & 0 & -\frac{\sqrt{2}}{2} & 0 \end{pmatrix}. \quad (38.78)$$

Notice that changing the contact models is easily accomplished by removing more rows. Changing contact 1 to HF would eliminate the fourth rows from \mathbf{G}^T and \mathbf{J} . Changing it to Pwof would eliminate the second, third and fourth rows of \mathbf{G}^T and \mathbf{J} . Changing the model at contact 2 would remove either just the eighth row or the sixth, seventh, and eighth rows.

Example 1, Part 3: Reduce to Planar Case

The grasp shown in Fig. 38.12 can be reduced to a planar problem by following the explicit formulas given above, but it can also be done by understanding the physical interpretations of the various rows and columns of the matrices. Proceed by eliminating velocities and forces that are out of the plane. This can be done by removing the z -axes from $\{\mathbf{N}\}$ and $\{\mathbf{B}\}$, and the $\hat{\mathbf{o}}$ -directions at the contacts. Further, joints 3 and 4 must be locked. The resulting \mathbf{G}^T and \mathbf{J} are constructed eliminating certain rows and columns. \mathbf{G}^T is formed by removing rows 3, 4, 7, and 8 and columns 3, 4, and 5. \mathbf{J} is formed by removing rows 3, 4, 7, and 8 and columns 3 and 4 yielding

$$\mathbf{G}^T = \begin{pmatrix} -c_1 & -s_1 & 0 \\ s_1 & -c_1 & -r \\ -c_2 & -s_2 & 0 \\ s_2 & -c_2 & -r \end{pmatrix}, \quad (38.79)$$

$$\mathbf{J} = \begin{pmatrix} -l_1 & -l_3 & 0 \\ l_2 & l_7 & 0 \\ 0 & 0 & 0 \\ 0 & 0 & l_6 \end{pmatrix}. \quad (38.80)$$

Example 1, Part 4: Grasp Classes

The first column of Table 38.11 reports the dimensions of the main subspaces of \mathbf{J} and \mathbf{G} for the sphere grasping example with different contact models. Only non-trivial null spaces are listed.

In the case of two HF contact models, all four null spaces are non-trivial, so the system satisfies the conditions for all four grasp classes. The system is graspable because there is an internal force along the line segment connecting the two contact points. Indeterminacy is manifested in the fact that the hand cannot resist a moment acting about that line. Redundancy is seen to exist since joint 3 can be used to move contact 2 out of the plane of the figure, but joint 4 can be rotated in the opposite direction to cancel this motion. Finally, the grasp is defective, because the contact forces and the instantaneous velocities along the $\hat{\mathbf{o}}_1$ and $\hat{\mathbf{n}}_2$ directions of contact 1 and 2, respectively, cannot be controlled through the joint torques and velocities. These interpretations are borne out in the null space basis matrices below, computed using $r = 1$, $\cos(\theta_1) = -0.8 = -\cos(\theta_2)$, $\sin(\theta_1) = \cos(\theta_2) = -0.6$, $l_1 = 3$, $l_2 = 2$, $l_3 = 1$, $l_4 = 2$, $l_5 = 1$, $l_6 = 1$, and $l_7 = 0$

$$\mathbf{N}(\mathbf{J}) \approx \begin{pmatrix} 0 \\ 0 \\ -0.73 \\ 0.69 \\ 0 \end{pmatrix}, \quad \mathbf{N}(\mathbf{G}^T) \approx \begin{pmatrix} 0 \\ 0 \\ 0.51 \\ 0.86 \\ 0 \\ 0 \end{pmatrix}, \quad (38.81)$$

$$\mathbf{N}(\mathbf{G}) \approx \begin{pmatrix} 0.57 \\ -0.42 \\ 0 \\ 0.57 \\ 0.42 \\ 0 \end{pmatrix}, \quad \mathbf{N}(\mathbf{J}^T) = \begin{pmatrix} 0 & 0 \\ 0 & 0 \\ 0 & -1 \\ 1 & 0 \\ 0 & 0 \\ 0 & 0 \end{pmatrix}. \quad (38.82)$$

Table 38.11 Dimensions of main subspaces and classifications of grasp studied in Example 1

Models	Dimension	Class
HF,HF	$\dim \mathcal{N}(\mathbf{J}) = 1$	Redundant
	$\dim \mathcal{N}(\mathbf{G}^T) = 1$	Indeterminate
	$\dim \mathcal{N}(\mathbf{G}) = 1$	Graspable
	$\dim \mathcal{N}(\mathbf{J}^T) = 2$	Defective
SF,HF	$\dim \mathcal{N}(\mathbf{J}) = 1$	Redundant
	$\dim \mathcal{N}(\mathbf{G}) = 1$	Graspable
	$\dim \mathcal{N}(\mathbf{J}^T) = 3$	Defective
HF,SF	$\dim \mathcal{N}(\mathbf{G}) = 1$	Graspable
	$\dim \mathcal{N}(\mathbf{J}^T) = 2$	Defective
SF,SF	$\dim \mathcal{N}(\mathbf{G}) = 2$	Graspable
	$\dim \mathcal{N}(\mathbf{J}^T) = 3$	Defective

Notice that changing either contact to SF makes it possible for the hand to resist external moments applied about the line containing the contacts, so the grasp loses indeterminacy, but retains graspability (with squeezing still possible along the line of the contacts). However, if contact 2 is the SF contact, the grasp loses its redundancy. While the second contact point can still be moved out of the plane by joint 3 and back in by joint 4, this canceled translation of the contact point yields a net rotation about \hat{n}_2 (this also implies that the hand can control the moment applied to the object along the line containing the contacts). Changing to SF at contact 2 does *not* affect the hand's inability to move contact 1 and contact 2 in the \hat{o}_1 and \hat{n}_2 directions, so the defectivity property is retained.

Example 1, Part 5: Desirable Properties

Assuming contact model types of SF and HF at contacts 1 and 2, respectively, \mathbf{G} is full row rank and so $\mathcal{N}(\mathbf{G}^T) = \mathbf{0}$ (see Table in part 4 of this example). Therefore, as long as the hand is sufficiently dexterous, it can apply any wrench in \mathbb{R}^6 to the object. Also, if the joints are locked, object motion will be prevented. Assuming the same problem values used in the previous part of this problem, the matrix \mathbf{G}^T is

$$\mathbf{G}^T = \begin{pmatrix} -c_1 & -s_1 & 0 & 0 & 0 & 0 \\ s_1 & -c_1 & 0 & 0 & 0 & -r \\ 0 & 0 & 1 & rs_1 & -rc_1 & 0 \\ 0 & 0 & 0 & -c_1 & -s_1 & 0 \\ \hline -c_2 & -s_2 & 0 & 0 & 0 & 0 \\ s_2 & -c_2 & 0 & 0 & 0 & -r \\ 0 & 0 & 1 & rs_2 & -rc_2 & 0 \end{pmatrix} \quad (38.83)$$

Bases for the three non-trivial null spaces are

$$\mathbf{N}(\mathbf{J}^T) = \begin{pmatrix} 0 & 0 & 0 \\ 0 & 0 & 0 \\ 0 & 0 & -1 \\ 1 & 0 & 0 \\ 0 & -1 & 0 \\ 0 & 0 & 0 \\ 0 & 0 & 0 \end{pmatrix}, \quad (38.84)$$

$$\mathbf{N}(\mathbf{J}) \approx \begin{pmatrix} 0 \\ 0 \\ -0.73 \\ 0.69 \\ 0 \end{pmatrix}, \quad \mathbf{N}(\mathbf{G}) \approx \begin{pmatrix} 0.57 \\ -0.42 \\ 0 \\ 0 \\ 0.57 \\ 0.42 \\ 0 \end{pmatrix}. \quad (38.85)$$

Since $\mathcal{R}(\mathbf{J})$ is four-dimensional and $\mathcal{N}(\mathbf{G})$ is one-dimensional, the maximum dimension of $\mathcal{R}(\mathbf{J}) + \mathcal{N}(\mathbf{G})$ cannot be more than 5, and therefore, the hand cannot control all possible object velocities. For example, the contact velocity $\mathbf{v}_{cc} = (0 \ 0 \ 0 \ 0.8 \ 0 \ 0)^T$ is in $\mathcal{N}(\mathbf{J}^T)$, and so cannot be controlled by the fingers. It is also equal to 0.6 times the third column of \mathbf{G}^T plus the 4th column of \mathbf{G}^T and therefore is in $\mathcal{R}(\mathbf{G}^T)$. Since the mapping between $\mathcal{R}(\mathbf{G})$ and $\mathcal{R}(\mathbf{G}^T)$ is one-to-one and onto, this uncontrollable contact velocity corresponds to a unique uncontrollable object velocity, $\mathbf{v} = (0 \ 0 \ 0.6 \ 1 \ 0 \ 0)$. In other words, the hand cannot cause the center of the sphere to translate in the z -direction, while also rotating about the x -axis (and not other axes simultaneously).

On the question of controlling all internal object forces, the answer is *yes*, since $\mathcal{N}(\mathbf{J}^T) \cap \mathcal{N}(\mathbf{G}) = \mathbf{0}$. This conclusion is clear from the fact that $\mathcal{N}(\mathbf{G})$ has non-zero values in the first, second, and sixth positions, while all columns of $\mathcal{N}(\mathbf{J}^T)$ have zeros in those positions.

Example 1, Part 6: Force Closure

Again assume that contacts 1 and 2 on the grasped sphere were modeled as SF and HF contacts, respectively. Under this assumption, \mathbf{G} is full row rank, and the internal force corresponds to equal and opposite contact forces. For frictional form closure to exist, the internal force must lie within the friction cones. Choosing r and the sines and cosines of θ_1 and θ_2 as in example 1, part 4, frictional form closure can be shown to exist if both friction coefficients are greater than 0.75. For this grasp, since $\mathcal{N}(\mathbf{J}^T) \cap \mathcal{N}(\mathbf{G}) = \mathbf{0}$, frictional form closure is equivalent to force closure.

The plot in Fig. 38.14 was generated by fixing μ_2 at a specific value and varying μ_1 from 0.5 to 2.0. Notice that for $\mu_1 < 0.75$, force closure does not exist regardless of the value of μ_2 . The metric increases smoothly until a specific value of μ_1 . From that point on, the friction coefficient at contact 2 is the limiting factor. To increase the metric further, μ_2 must be increased.

38.5.2 Example 2: Grasped Polygon in the Plane

Part 1: \mathbf{G} and \mathbf{J}

Figure 38.15 shows a planar hand grasping a polygon. Finger 1 (on the right) contains two joints numbered 1 and 2. Finger 2 contains joints 3–7, which are numbered in increasing order moving from the palm distally. The inertial frame has been chosen to lie inside the object, with its x -axis passing through contacts 1 and 2, and collinear with the normal vector of contact 2.

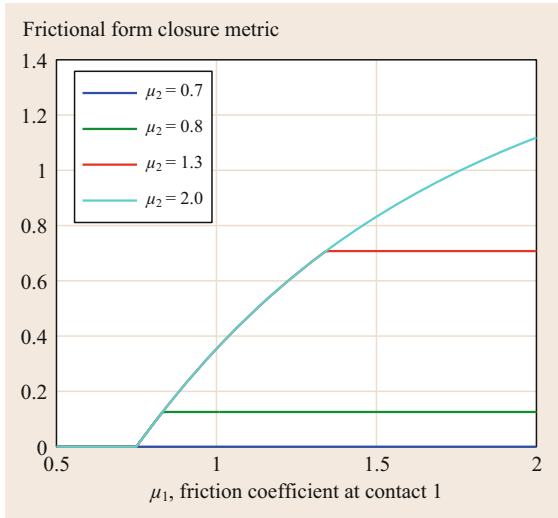


Fig. 38.14 Plot of force closure metric versus friction coefficient on contact 1

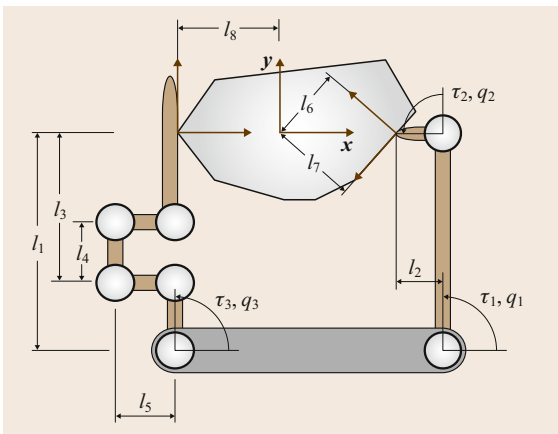


Fig. 38.15 Planar hand with 2 fingers and 7 joints grasping a polygonal object

The rotation matrices are given by

$$\mathbf{R}_1 = \begin{pmatrix} -0.8 & -0.6 \\ 0.6 & -0.8 \end{pmatrix}, \quad \mathbf{R}_2 = \begin{pmatrix} 1 & 0 \\ 0 & 1 \end{pmatrix}. \quad (38.86)$$

Assuming HF contacts, \mathbf{G} is given as follows

$$\mathbf{G} = \begin{pmatrix} -0.8 & -0.6 & 1 & 0 \\ 0.6 & -0.8 & 0 & 1 \\ l_6 & -l_7 & 0 & -l_8 \end{pmatrix}. \quad (38.87)$$

Notice that the first two columns of \mathbf{G} correspond to the normal and tangential unit vectors at contact 1. The third and fourth columns correspond to contact 2.

Assuming HF contacts and all joints are active (i. e., not locked), \mathbf{J} is

$$\mathbf{J}^T = \begin{pmatrix} 0.8l_1 & 0.6l_1 & \mathbf{0} \\ -0.6l_2 & 0.8l_2 & \mathbf{0} \\ \mathbf{0} & -l_1 & 0 \\ & -l_3 & 0 \\ & -l_3 & l_5 \\ & -l_3 + l_4 & l_5 \\ & -l_3 + l_4 & 0 \end{pmatrix}. \quad (38.88)$$

The first two columns of \mathbf{J}^T are the torques required to produce a unit force in the $\hat{\mathbf{n}}_1$ and $\hat{\mathbf{t}}_1$ directions at contact 1. The horizontal line through the matrix partitions the contributions for the first finger (the upper part) and second finger. Notice that both \mathbf{J}^T and \mathbf{G} are full column rank.

Example 2, Part 2: Grasp Classes

This example clearly illustrates the physical qualities of the various grasp classes without introducing features that can cloud the descriptions.

We now discuss the details of the four grasp classes using the previous planar example. During these discussions it is useful to choose non-dimensional values for the parameters in the grasping system. The lengths were assumed to have the following values (the results are the same, regardless of a particular choice of units, so units are not specified)

$$l_1 = 2.89, \quad l_2 = 0.75, \quad l_3 = 1.97, \quad (38.89)$$

$$l_4 = 0.80, \quad l_5 = 0.80, \quad l_6 = 0.90, \quad (38.90)$$

$$l_7 = 1.20, \quad l_8 = 1.35. \quad (38.91)$$

Redundant. Redundancy exists if $\mathcal{N}(\mathbf{J})$ is non-trivial. Assuming that both contacts are hard contacts and all the joints are active, $\text{rank}(\mathbf{J}) = 4$, so $\mathcal{N}(\mathbf{J})$ is three-dimensional. A basis for $\mathcal{N}(\mathbf{J})$ was obtained using Matlab's `null()` function

$$\mathbf{N}(\mathbf{J}) \approx \begin{pmatrix} 0 & 0 & 0 \\ 0 & 0 & 0 \\ -0.49 & -0.31 & -0.27 \\ 0.53 & 0.64 & -0.17 \\ 0.49 & -0.50 & -0.02 \\ -0.49 & 0.50 & 0.02 \\ -0.02 & 0.01 & 0.95 \end{pmatrix}. \quad (38.92)$$

Since the first two rows are zero, $\mathcal{N}(\mathbf{J})$ does not include motions of the first finger (on the right of the palm). To understand this, assume the object is fixed in the plane. Then the first finger cannot maintain sticking contact at contact 1 unless its joints are also fixed.

The three non-zero columns corresponding to finger 2 show that there are 3 basis motions of its joints that allow the finger contact to stick to the object contact. For example, the first column shows that if joint 3 moves roughly as much as joints 4, 5, and 6, but in the opposite direction as joints 4 and 5 and in the same direction as joint 6, while joint 7 is more or less fixed, then contact 2 will be maintained.

Notice that finger 2 contains a parallelogram. Because of this geometry, one can see that the vector $(0\ 0\ 0\ -1\ 1\ -1\ 1)^T$ is an element of $\mathcal{N}(\mathbf{J})$. The velocity interpretation of this vector is that the link of the finger connected to the palm, and the link touching the object remain fixed in space, while the parallelogram moves as a simple four-bar mechanism. Similarly, joint actions in $\mathcal{N}(\mathbf{J})$ do not affect the contact forces, but cause internal hand velocities. Also, notice that since $\mathcal{N}(\mathbf{J}^T) = \mathbf{0}$, the entire space of possible generalized velocities and forces at the contacts can be generated by the joints.

Indeterminate. As noted above, with HF contact models, the system is graspable. However, replacing the HF models with PwoF models removes the tangent force components in the \hat{i}_1 and \hat{i}_2 directions. This effectively removes columns 2 and 4 from \mathbf{G} , which guarantees that the system will be indeterminate. The reduced matrix is denoted by $\mathbf{G}_{(1,3)}$. In this case $\mathcal{N}(\mathbf{G}_{(1,3)}^T)$ is

$$\mathbf{N}(\mathbf{G}_{(1,3)}^T) \approx \begin{pmatrix} 0 \\ -0.83 \\ 0.55 \end{pmatrix}. \quad (38.93)$$

Physically, this basis vector corresponds to moving the object such that the point coincident with the origin of $\{\mathbf{N}\}$ moves directly downward, while the object rotates counter clockwise. Also, if the analogous force and moment were applied to the object, the frictionless contacts could not maintain equilibrium.

Graspable. With two HF contact models in force, $\text{rank}(\mathbf{G}) = 3$, so $\mathcal{N}(\mathbf{G})$ is one-dimensional and the system is graspable. The null space basis vector of the grasp matrix is

$$\mathbf{N}(\mathbf{G}) \approx \begin{pmatrix} 0.57 \\ 0.42 \\ 0.71 \\ 0 \end{pmatrix}. \quad (38.94)$$

The physical interpretation of this basis vector is two opposing forces acting through the two contact points.

Recall that because the contact model is kinematic, there is no consideration of contact friction. However, given the direction of the contact normal relative to the line of the internal force, one can see that if the coefficient of friction is not greater than 0.75, squeezing tightly will cause sliding at contact 1, thus violating the kinematic contact model.

Defective. In a defective grasp, $\mathcal{N}(\mathbf{J}^T) \neq \mathbf{0}$. Given that the original \mathbf{J} is full row rank, the grasp is *not* defective. However, it can be made defective by locking a number of joints and/or changing the hand's configuration so that \mathbf{J} is no longer full rank. For example, locking joints 4, 5, 6, and 7 makes finger 2 a single-link finger with only joint 3 active. In this new grasping system, $\mathbf{J}_{(1,2,3)}^T$ is simply the first three rows of the original \mathbf{J}^T given in (38.88), where the subscript is the list of indices of active joints. The null space basis vector is

$$\mathbf{N}(\mathbf{J}_{(1,2,3)}^T) = \begin{pmatrix} 0 \\ 0 \\ 0 \\ 1 \end{pmatrix}. \quad (38.95)$$

This grasp is defective, since there is a subspace of contact velocities and forces that cannot be controlled by joint generalized velocities and forces. Since only the last component of $\mathbf{N}(\mathbf{J}_{(1,2,3)}^T)$ is non-zero, it would be impossible for the hand to give the contact point 2 on the object a velocity in the \hat{i}_2 -direction while maintaining the contact. This is also clear from the arrangement of joint 3, contact 2, and the direction of the contact normal. The dual interpretation is that forces in $\mathcal{N}(\mathbf{J}^T)$ are resisted by the structure and the corresponding joint loads is zero, or equivalently that those forces are not controllable by the hand. Notice that if the model of contact 2 were changed to point-without-friction, then $\mathbf{N}(\mathbf{J}_{(1,2,3)}^T) = \mathbf{0}$ and the system would no longer be defective.

38.5.3 Example 3: Hyperstatic Grasps

Part 1: $\tilde{\mathbf{G}}$ and $\tilde{\mathbf{J}}$

Figure 38.16 shows a planar projection of a three-dimensional sphere of radius l grasped by one finger only, with 3 revolute joints, through 3 contacts. The frames $\{\mathbf{C}\}_1$, $\{\mathbf{C}\}_2$ and $\{\mathbf{C}\}_3$ are oriented so that their \hat{o} -directions point out of the plane of the figure (as indicated by the small filled circle). The axes of the frames $\{\mathbf{N}\}$ and $\{\mathbf{B}\}$ were chosen to be axis-aligned with coincident origins located at the center of the sphere. The z -axes are pointing out of the page. Observe that since

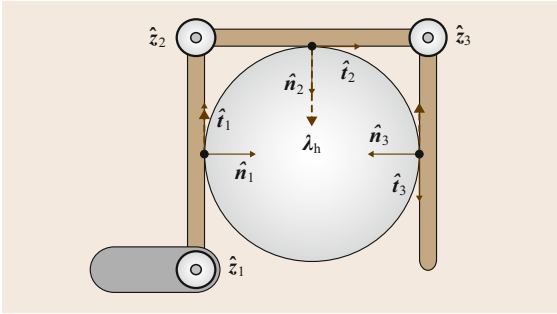


Fig. 38.16 A sphere grasped by a finger with three revolute joints. The force direction λ_h (dashed line) is a force that belongs to both $\mathcal{N}(\mathbf{G})$ and $\mathcal{N}(\mathbf{J}^T)$ and causes hyperstaticity

the three joint axes of the finger are perpendicular to the (x, y) -plane, the grasp operates in that plane for all time.

Assume that the width of all the links of the robotic hand is zero. Rotation matrices \mathbf{R}_i and vectors $\mathbf{c}_i - \mathbf{p}$ for $i = 1, \dots, 3$, can be computed as in (38.66) and (38.67) considering that $\theta_1 = \pi$, for contact 1, $\theta_2 = \pi/2$ and $\theta_3 = 0$, for contact 2 and 3, respectively. Finally, the complete grasp matrix is

$$\tilde{\mathbf{G}}^T = (\tilde{\mathbf{G}}_1 \quad \tilde{\mathbf{G}}_2 \quad \tilde{\mathbf{G}}_3)^T \in \mathbb{R}^{18 \times 6},$$

where $\tilde{\mathbf{G}}_i$ is as defined in (38.68)

$$\tilde{\mathbf{G}}^T = \begin{pmatrix} 1 & 0 & 0 & 0 & 0 & 0 \\ 0 & 1 & 0 & 0 & 0 & -l \\ 0 & 0 & 1 & 0 & l & 0 \\ 0 & 0 & 0 & 1 & 0 & 0 \\ 0 & 0 & 0 & 0 & 1 & 0 \\ 0 & 0 & 0 & 0 & 0 & 1 \\ \hline 0 & -1 & 0 & 0 & 0 & 0 \\ 1 & 0 & 0 & 0 & 0 & -l \\ 0 & 0 & 1 & l & 0 & 0 \\ 0 & 0 & 0 & 0 & -1 & 0 \\ 0 & 0 & 0 & 1 & 0 & 0 \\ 0 & 0 & 0 & 0 & 0 & 1 \\ \hline -1 & 0 & 0 & 0 & 0 & 0 \\ 0 & -1 & 0 & 0 & 0 & -l \\ 0 & 0 & 1 & 0 & -l & 0 \\ 0 & 0 & 0 & -1 & 0 & 0 \\ 0 & 0 & 0 & 0 & -1 & 0 \\ 0 & 0 & 0 & 0 & 0 & 1 \end{pmatrix}$$

Construction of the complete hand Jacobian $\tilde{\mathbf{J}}_i$ for contact i requires knowledge of the joint axis directions and

the origins of the frames fixed to the links of each finger. Assume that the origins of the Denavit–Hartenberg (DH) frames lie in the plane of the figure. In the current configuration, the quantities of interest for contact 1, expressed directly in $\{\mathcal{N}\}$ are

$$\begin{aligned} \mathbf{c}_1 - \boldsymbol{\zeta}_1 &= (0 \quad l \quad 0)^T, \\ \hat{\mathbf{z}}_1 &= (0 \quad 0 \quad 1)^T. \end{aligned}$$

The quantities of interest for contact 2, in $\{\mathcal{N}\}$ are

$$\begin{aligned} \mathbf{c}_2 - \boldsymbol{\zeta}_1 &= (l \quad 2l \quad 0)^T, \\ \mathbf{c}_2 - \boldsymbol{\zeta}_2 &= (l \quad 0 \quad 0)^T, \\ \hat{\mathbf{z}}_1 &= (0 \quad 0 \quad 1)^T, \\ \hat{\mathbf{z}}_2 &= (0 \quad 0 \quad 1)^T. \end{aligned}$$

The quantities of interest for contact 3, in $\{\mathcal{N}\}$ are

$$\begin{aligned} \mathbf{c}_3 - \boldsymbol{\zeta}_1 &= (2l \quad l \quad 0)^T, \\ \mathbf{c}_3 - \boldsymbol{\zeta}_2 &= (2l \quad -l \quad 0)^T, \\ \mathbf{c}_3 - \boldsymbol{\zeta}_3 &= (0 \quad -l \quad 0)^T, \\ \hat{\mathbf{z}}_1 &= (0 \quad 0 \quad 1)^T, \\ \hat{\mathbf{z}}_2 &= (0 \quad 0 \quad 1)^T, \\ \hat{\mathbf{z}}_3 &= (0 \quad 0 \quad 1)^T. \end{aligned}$$

The complete hand Jacobian $\tilde{\mathbf{J}} \in \mathbb{R}^{18 \times 3}$ (contact velocities are expressed in $\{\mathcal{C}\}_i$) is

$$\tilde{\mathbf{J}} = \begin{pmatrix} -l & 0 & 0 \\ 0 & 0 & 0 \\ 0 & 0 & 0 \\ 0 & 0 & 0 \\ 0 & 0 & 0 \\ 1 & 0 & 0 \\ \hline -l & -l & 0 \\ -2l & 0 & 0 \\ 0 & 0 & 0 \\ 0 & 0 & 0 \\ 0 & 0 & 0 \\ 0 & 0 & 0 \\ 1 & 1 & 0 \\ \hline l & -l & -l \\ -2l & -2l & 0 \\ 0 & 0 & 0 \\ 0 & 0 & 0 \\ 0 & 0 & 0 \\ 1 & 1 & 1 \end{pmatrix}.$$

The horizontal dividing lines partition $\tilde{\mathbf{J}}$ into $\tilde{\mathbf{J}}_1$ (on top), $\tilde{\mathbf{J}}_2$, and $\tilde{\mathbf{J}}_3$ (on the bottom). The columns correspond to joints 1 through 3.

Example 3, Part 2: \mathbf{G} and \mathbf{J}

Assume that the 3 contacts in Fig. 38.16 are of type HF. Then the selection matrix \mathbf{H} is given by

$$\mathbf{H} = \begin{pmatrix} \mathbf{I} & \mathbf{0} & \mathbf{0} & \mathbf{0} & \mathbf{0} & \mathbf{0} \\ \mathbf{0} & \mathbf{0} & \mathbf{I} & \mathbf{0} & \mathbf{0} & \mathbf{0} \\ \mathbf{0} & \mathbf{0} & \mathbf{0} & \mathbf{0} & \mathbf{I} & \mathbf{0} \end{pmatrix}, \quad (38.96)$$

where \mathbf{I} and $\mathbf{0}$ are in $\mathbb{R}^{3 \times 3}$, thus matrices $\mathbf{G}^T \in \mathbb{R}^{9 \times 6}$ and $\mathbf{J} \in \mathbb{R}^{9 \times 3}$ are obtained by removing rows related to rotations from $\tilde{\mathbf{G}}^T$ and $\tilde{\mathbf{J}}$

$$\mathbf{G}^T = \begin{pmatrix} 1 & 0 & 0 & 0 & 0 & 0 \\ 0 & 1 & 0 & 0 & 0 & -l \\ 0 & 0 & 1 & 0 & l & 0 \\ \hline 0 & -1 & 0 & 0 & 0 & 0 \\ 1 & 0 & 0 & 0 & 0 & -l \\ 0 & 0 & 1 & l & 0 & 0 \\ \hline -1 & 0 & 0 & 0 & 0 & 0 \\ 0 & -1 & 0 & 0 & 0 & -l \\ 0 & 0 & 1 & 0 & -l & 0 \end{pmatrix},$$

$$\mathbf{J} = \begin{pmatrix} l & 0 & 0 \\ 0 & 0 & 0 \\ 0 & 0 & 0 \\ \hline l & l & 0 \\ 2l & 0 & 0 \\ 0 & 0 & 0 \\ \hline l & l & l \\ 2l & 2l & 0 \\ 0 & 0 & 0 \end{pmatrix}.$$

Example 3, Part 3: Grasp Classes

The first column of Table 38.12 reports the dimensions of the main subspaces of \mathbf{J}^T and \mathbf{G} for the sphere grasping example with three hard finger contacts. Only non-trivial null spaces are listed.

The system is defective because there are generalized contact forces belonging to the subspace that are resisted by the structure, which correspond to zero joint

Table 38.12 Dimensions of main subspaces and classification of grasp given in Example 3

Dimension	Class
$\dim \mathcal{N}(\mathbf{J}^T) = 6$	Defective
$\dim \mathcal{N}(\mathbf{G}) = 3$	Graspable
$\dim \mathcal{N}(\mathbf{J}^T) \cap \mathcal{N}(\mathbf{G}) = 1$	Hyperstatic

actions

$$\mathbf{N}(\mathbf{J}^T) = \begin{pmatrix} 0 & 0 & 0 & 0 & -2 & 0 \\ 0 & 0 & 0 & 1 & 0 & 0 \\ 0 & 0 & 1 & 0 & 0 & 0 \\ \hline 0 & 0 & 0 & 0 & 0 & -2 \\ 0 & 0 & 0 & 0 & 1 & 0 \\ 0 & 1 & 0 & 0 & 0 & 0 \\ \hline 0 & 0 & 0 & 0 & 0 & 0 \\ 0 & 0 & 0 & 0 & 0 & 1 \\ 1 & 0 & 0 & 0 & 0 & 0 \end{pmatrix}.$$

The first three columns represent generalized forces acting at the three contact points in a direction perpendicular to the plane of the Fig. 38.16. The fourth column corresponds to a contact force applied only along the \hat{t}_1 direction.

System is graspable because the subspace of internal forces is three-dimensional; a possible basis matrix is

$$\mathbf{N}(\mathbf{G}) = \begin{pmatrix} 1 & 1 & 0 \\ 1 & 0 & 1 \\ 0 & 0 & 0 \\ \hline 1 & 0 & 2 \\ -1 & 0 & 0 \\ 0 & 0 & 0 \\ \hline 0 & 1 & 0 \\ 0 & 0 & -1 \\ 0 & 0 & 0 \end{pmatrix}.$$

The three force vectors of subspace $\mathbf{N}(\mathbf{G})$ are easily identified from Fig. 38.16. Note that all forces are expressed in local contact frames. The first column vector of $\mathbf{N}(\mathbf{G})$ represents opposed forces at contacts 1 and 2 along the line joining contacts 1 and 2. The second column vector parameterizes opposed forces at contacts 1 and 3 along the line joining contacts 1 and 3. The last vector represents forces along direction λ_h , shown as the (dashed lines) in Fig. 38.16. Note that this direction (in wrench intensity space) corresponds to two upward friction forces at the left and right contacts and one downward with double the magnitude from the center of the top link in the work space.

Finally, the grasp is hyperstatic because

$$\mathbf{N}(\mathbf{G}) \cap \mathbf{N}(\mathbf{J}^T) = \begin{pmatrix} 0 \\ 1 \\ 0 \\ 2 \\ 0 \\ 0 \\ 0 \\ -1 \\ 0 \end{pmatrix} \neq 0.$$

Hyperstatic forces in this subspace, are internal forces that cannot be controlled through the hand joints. In Fig. 38.16 the internal force λ_h that is also in $\mathbf{N}(\mathbf{J}^T)$ is reported.

The grasp in Fig. 38.16 is an example of *power grasp*, style of grasp mentioned earlier that uses many contact points not only on the fingertips but also on the links of fingers and the palm [38.8, 28, 33].

All power grasps are kinematically defective ($\mathcal{N}(\mathbf{J}^T) \neq \mathbf{0}$) and usually are hyperstatic. According to Sect. 38.2.2, rigid-body modeling is not sufficient to capture the overall system behavior, because the generalized contact forces in $\mathcal{N}(\mathbf{G}) \cap \mathcal{N}(\mathbf{J}^T)$ leave the dynamics indeterminate.

Many approaches have been used to overcome rigid-body limitation in hyperstatic grasps such as those proposed in [38.16, 20, 21] where visco-elastic contact models have been used to solve the force indeterminacy. In [38.48], authors found that a sufficient condition for hyperstaticity is $m > q + 6$ where m is the dimension of contact force vector.

38.5.4 Example 4: Duality

Consider a frictionless disc constrained to translate in the plane; (Fig. 38.17). In this problem $n_v = 2$, so the space of applied contact forces and object velocities is

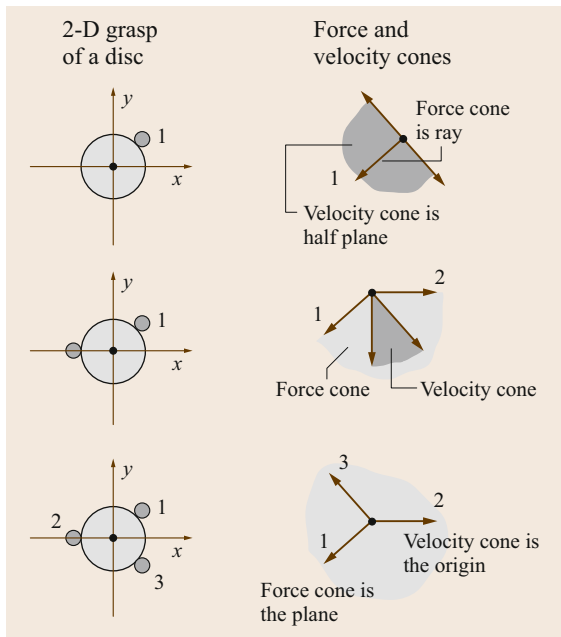


Fig. 38.17 Case of a translating disc in the plane: Relationship between frictionless contacts and possible disc velocities and net contact forces

the plane \mathbb{R}^2 . In the top pair of pictures, a single (fixed) contact point imposes a half space constraint on the instantaneous velocity and limits the force at a frictionless contact to the ray. Both the ray and the (dark gray) half space are defined by the contact normal pointing into the object. Notice that the ray and half space are dual cones. When two contacts are present, the (light gray) force cone becomes the non-negative span of the two contact normals and the velocity cone is its dual. With the addition of the third contact, the grasp has form closure as indicated by the degeneration of the velocity cone to the origin and the expansion of the force cone to become equal to the plane.

It is important to point out that the discussion of the dual cones applies to three-dimensional bodies after replacing the contact normals with the columns of \mathbf{G} .

38.5.5 Example 5: Form Closure

Part 1: Unilateral Constraints

Form closure of a spatial object requires seven unilateral contacts, which is difficult to illustrate. Therefore, the only form closure example analyzed in this chapter is the planar problem shown in Fig. 38.18. In the plane only four unilateral contacts are needed. In this problem, even though the fourth contact is at a vertex of the object, the contact normal is still well-defined. The angle α of the finger is allowed to vary, and it can be shown that form closure exists if α lies in the interval: $1.0518 < \alpha < \frac{\pi}{2}$. Notice that a critical value of α occurs when the lower edge of C_2 contains contact point 3 ($\alpha \approx 1.0518$) and contact point 2 ($\alpha = \frac{\pi}{2}$). Beyond these angles, the cone C_1 and C_2 can no longer see each other.

Choosing the frame for analysis with origin at the fourth contact point, the grasp matrix for this example

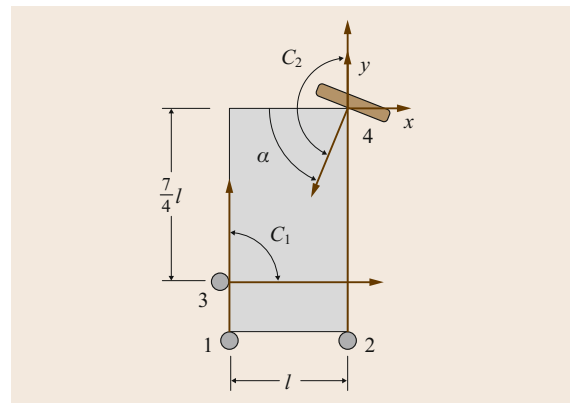


Fig. 38.18 Plot of closure metrics versus angle of contact for $1.04 < \alpha < 1.59$

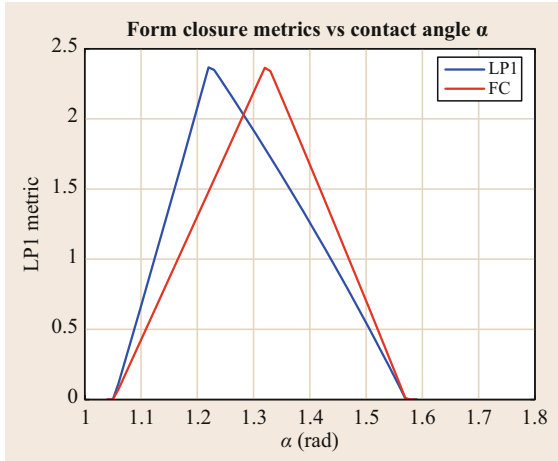


Fig. 38.19 Planar grasp with first-order form closure if $1.052 < \alpha < \frac{\pi}{2}$

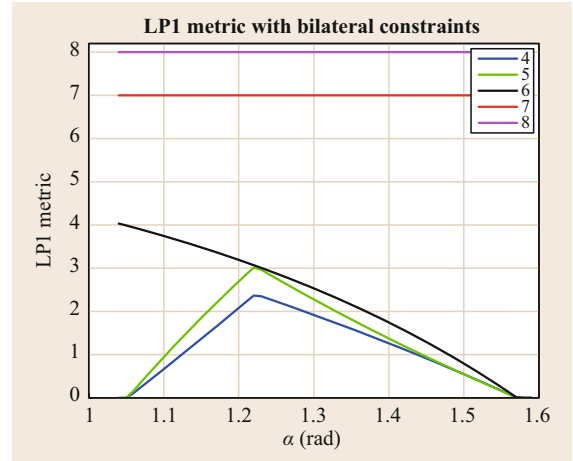


Fig. 38.20 First-order form closure metric for Fig. 38.18 with progressively more contacts converted to bilateral

is

$$\mathbf{G} = \begin{pmatrix} 0 & 0 & 1 & -\cos(\alpha) \\ 1 & 1 & 0 & -\sin(\alpha) \\ -l & 0 & \frac{7}{4}l & 0 \end{pmatrix}. \quad (38.97)$$

Form closure was tested for a range of angles. The blue curve in Fig. 38.19 is the LP1 metric ($d^* * n_c$ returned by the function `formClosure.m`, available from [38.43]), which indicates that the grasp farthest from losing form closure has $\alpha \approx 1.222$ radians, which is the configuration shown in Fig. 38.18. For comparison purposes, the Ferrari–Canny metric (scaled to have the same maximum as the LP1 metric) is plotted in red. They agree on the angles for which form closure exists, but differ on the optimal α .

Example 5, Part 2: Bilateral Constraints

Let us next consider form closure with a mix of bilateral and unilateral constraints using (38.54). For example, if contact 1 is treated as a bilateral constraint and the remaining are considered to be unilateral, \mathbf{G}_n and \mathbf{B} are

$$\mathbf{B} = \begin{pmatrix} 0 \\ 1 \\ -l \end{pmatrix}, \quad \mathbf{G}_n = \begin{pmatrix} 0 & 1 & -\cos(\alpha) \\ 1 & 0 & -\sin(\alpha) \\ 0 & \frac{7}{4}l & 0 \end{pmatrix}. \quad (38.98)$$

Additional contacts can be converted to bilateral by moving their corresponding columns from \mathbf{G}_n to \mathbf{B} . Figure 38.20 shows five plots of the form closure metric LP1. In the legend, 4 refers to the grasp with all four contacts treated as unilateral, 5 means that contact 1 has been converted to bilateral as defined by the previous equation, 6 means that contacts 1 and 2 have been

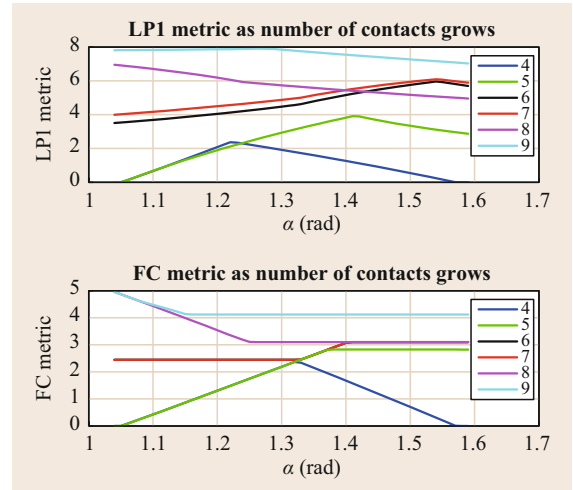


Fig. 38.21 Comparison of the monotonicity properties of the LP1 and Ferrari–Canny form closure metrics

converted to bilateral, etc. The plots show an important property of the LP1 metric; the maximum value is equal to the number of unilateral contacts (bilateral contacts count as two unilateral contacts), which is attained for curves 7 and 8. For this particular problem, these maxima are achieved for all α .

Example 5, Part 3: Monotonicity

If one were to zoom in on curves 4 and 5 near $\alpha = 1.5$, one would see that LP1 is not monotonic as constraints are added. That is, when contact 1 is converted from unilateral (curve 4) to bilateral (curve 5), for some values of α , the LP1 metric is smaller despite the additional constraint. To demonstrate monotonicity, the monotonic Ferrari–Canny metric and the non-monotonic LP1

metric were computed as a function of α for a sequence of grasps. Starting with the original four contacts, five unilateral contacts were added: $\{(0, -1.3l), (-0.5l, 0), (0, 1.75l), (-l, -0.6l), (-0.7l, 0)\}$. Figure 38.21 shows the metrics with 4, 5, 6, 7, 8, and 9 contacts, as indicated by the legend.

The LPI metric does not increase monotonically as contacts are added for every α . Near $\alpha = 1.2$ adding

the fifth contact reduces the metric slightly. Also, near $\alpha = 1.55$, adding the eighth contact reduces the metric. By contrast, the Ferrari–Canny metric is monotonic, although not strictly monotonic; the plots labeled 6 and 7 are identical for all α and there are other intervals of α where the metric is constant as contacts are added. For example, near $\alpha = 1.35$, the grasps with 5, 6, and 7 contacts all have the same metric value.

38.6 Conclusion and Further Reading

A great deal of understanding of grasping systems can be derived from the simple linear kinematic, dynamic, and contact models presented in this chapter. The most widely used grasp classifications and closure properties can all be derived from these models under the rigid-body assumption. Linearizing these models leads to metrics and tests that can be computed efficiently using computational linear algebra and linear programming techniques. Grasp synthesis tools built on these tests take object and hand models as inputs and return a set of possible grasp configurations as outputs (see for example [38.3]). In-depth discussions of grasp kinematics and grasp classifications can be found in [38.15, 20, 20, 34, 48–52].

One has to wonder what insights have been lost as a result of the simplifying assumptions made in this chapter. For the interested reader, there are a host of papers that analyze grasping systems under more sophisticated assumptions. In general, bodies are curved and compliant [38.17, 28, 35, 53–55] and contact friction models are not quite as simple as the linearized ones so widely adopted. For example, if a contact has to resist a moment about its normal, its effective tangential friction coefficient is reduced [38.46, 56]. In this chapter, the quadratic Coulomb friction cone was approximated by a polyhedral cone. The analysis problems are more difficult when using the quadratic cone, but they are quite tractable [38.47, 57].

In principle, a properly designed grasping system could be controlled to maintain all contacts, but worldly realities can lead to unwanted slipping or twisting. This leads us back to the topic of grasp stability, which is too often equated to grasp closure. However, grasp closure is really equivalent to the existence of equilibrium, which is a necessary, but not sufficient, condition for stability. The common definition of stability outside of the field of robotic grasping requires that when a system is deflected from an equilibrium point, the system returns to this point. From this perspective, and under the assumption of no slipping at the contact points, it is known that all closure grasps are stable, but

the converse is not necessarily true [38.53, 54, 58, 59]. However, stability analysis when contacts slide is still an open question.

Given a stable grasp, another important consideration not discussed in this chapter is that of grasp force distribution problem, i. e., finding *good* actuator torques and contact forces to balance a given external load applied to the object. This problem was studied in the context of walking machines first by *McGhee* and *Orin* [38.60] and later by several others [38.61, 62]. *Kumar* and *Waldron* applied similar techniques to force distribution problems in grasping [38.63]. Work by *Han* et al. and *Buss* et al. solved the force distribution problem with non-linear friction cone constraints by taking advantage of convex optimization techniques [38.47, 57, 64]. In power grasps, this problem of finding a good distribution is difficult, because the space of controllable contact wrenches is severely restricted by the large number of contacts [38.21, 32, 33, 65].

Grasp synthesis largely depends on the structure of the robotic hands that are often very complex systems with many degrees of freedom, sensors and actuators, which are necessary to adapt to many different objects and tasks. An important research area, not discussed in this chapter, is that of designing simplified hands coupling some of the degrees of freedom, reducing the number of effective inputs, and leading to more efficient, simpler and reliable designs [38.23, 66]. A reduction of independent inputs is observed also in human hand movement data, where few variables, defined as postural synergies, explain most of the variance in the configurations of the hand while grasping different objects [38.25, 67]. The reduction of the number of independently controlled inputs in the hand affects grasp properties, and in particular the ability of the hand to dexterously controlling grasp forces and in-hand manipulation as discussed in [38.68–71].

All of the above considerations implicitly assume that a grasp has been achieved, which is no easy task. The bulk of today’s research in robotic grasping can be fairly characterized as focused on *grasp acquisition*.


In other words, the problem is to move the hand from a state of no contact with the object to one in which a satisfactory grasp has been achieved. When a robot identifies an object to grasp, its knowledge of the object's pose and geometry are not perfect. Even if they were, the robot's control system could not move the hand perfectly to the desired grasping points. The hand will bump the object accidentally, altering its pose, possibly leading to grasp failure.

Areas of current research cover methods that exploit some detailed aspects of planned or sensed contact interactions that occur before achieving the final grasp and those that try to be robust to pre-grasp contact interactions. In the first category are quasistatic push-grasping, dynamic grasp acquisition, and perception. Push-grasping seeks out contact prior to wrapping the fingers in order to allow the object to settle into a good position against the palm. It has, so far, been applied to objects that can slide stably across a horizontal surface cluttered with object that are not to be grasped [38.72]. Dynamic planning combines a dynamic model of grasping that includes intermittent contact to design optimal controllers and grasping actions

simultaneously [38.73]. The performance of both of the above in real-time implementations could be improved by new grasp perception methods, which estimate the pose of the object relative to the hand [38.74–76].

Impedance controllers are being developed to reduce the negative effects of unexpected contacts between the hand and object as the grasp is being formed [38.77] and between the object and environment during object transport tasks [38.78]. Independent contact regions are surface patches on the object which have the property: if a contact point is stabilized anywhere inside each region, then the grasp will have force closure [38.79, 80]. With this approach, a small amount of jostling will not cause grasp failure. Perhaps caging takes the independent regions idea to the extreme. Here the goal is to find a configuration of the hand that loosely surrounds the object with the additional condition that the object cannot escape without deforming itself or the hand [38.81, 82]. The challenges in caging are in finding a pre-cage configuration and a finger motion plan that impose the least restrictive accuracy requirements on the robots perception and control systems.

Video-References

-  **VIDEO 551** Grasp analysis using the MATLAB toolbox SynGrasp available from <http://handbookofrobotics.org/view-chapter/04/videodetails/551>

References

- 38.1 A. Bicchi: Hands for dextrous manipulation and powerful grasping: A difficult road towards simplicity, *IEEE Trans. Robotics Autom.* **16**, 652–662 (2000)
- 38.2 J.K. Salisbury: Kinematic and Force Analysis of Articulated Hands, Ph.D. Thesis (Stanford University, Stanford 1982)
- 38.3 A.T. Miller, P.K. Allen: GraspIt! A versatile simulator for robotic grasping, *IEEE Robotics Autom. Mag.* **11**(4), 110–122 (2004)
- 38.4 M. Malvezzi, G. Gioioso, G. Salvietti, D. Prattichizzo: SynGrasp: A matlab toolbox for underactuated and compliant hands, *IEEE Robotics Autom. Mag.* **22**(4), 52–68 (2015)
- 38.5 M. Malvezzi, G. Gioioso, G. Salvietti, D. Prattichizzo, A. Bicchi: Syngrasp: A matlab toolbox for grasp analysis of human and robotic hands, *Proc. IEEE Int. Conf. Robotics Autom. (ICRA)* (2013) pp. 1088–1093
- 38.6 SynGrasp: A MATLAB Toolbox for Grasp Analysis of Human and Robotic Hands, <http://syngrasp.dii.unisi.it>
- 38.7 M. Grebenstein, A. Albu-Schäffer, T. Bahls, M. Chalou, O. Eiberger, W. Friedl, R. Gruber, S. Haddadin, U. Hagn, R. Haslinger, H. Hoppner, S. Jorg, M. Nickl, A. Nothhelfer, F. Petit, J. Reill, N. Seitz, T. Wimbock, S. Wolf, T. Wusthoff, G. Hirzinger: The DLR hand arm system, *IEEE Conf. Robotics Autom.* (2011) pp. 3175–3182
- 38.8 K. Salisbury, W. Townsend, B. Ebrman, D. DiPietro: Preliminary design of a whole-arm manipulation system (WAMS), *Proc. IEEE Int. Conf. Robotics Autom.* (1988) pp. 254–260
- 38.9 M.S. Ohwovoriole, B. Roth: An extension of screw theory, *J. Mech. Des.* **103**, 725–735 (1981)
- 38.10 K.H. Hunt: *Kinematic Geometry of Mechanisms* (Oxford Univ. Press, Oxford 1978)
- 38.11 T.R. Kane, D.A. Levinson, P.W. Likins: *Spacecraft Dynamics* (McGraw Hill, New York 1980)
- 38.12 J.J. Craig: *Introduction to Robotics: Mechanics and Control*, 2nd edn. (Addison-Wesley, Reading 1989)
- 38.13 J.K. Salisbury, B. Roth: Kinematic and force analysis of articulated mechanical hands, *J. Mech. Transm. Autom. Des.* **105**(1), 35–41 (1983)

- 38.14 M.T. Mason, J.K. Salisbury Jr: *Robot Hands and the Mechanics of Manipulation* (MIT Press, Cambridge 1985)
- 38.15 A. Bicchi: On the closure properties of robotic grasping, *Int. J. Robotics Res.* **14**(4), 319–334 (1995)
- 38.16 D. Prattichizzo, A. Bicchi: Consistent task specification for manipulation systems with general kinematics, *ASME J. Dyn. Syst. Meas. Control* **119**(4), 760–767 (1997)
- 38.17 J. Kerr, B. Roth: Analysis of multifingered hands, *Int. J. Robotics Res.* **4**(4), 3–17 (1986)
- 38.18 G. Strang: *Introduction to Linear Algebra* (Wellesley–Cambridge Press, Wellesley 1993)
- 38.19 R.M. Murray, Z. Li, S.S. Sastry: *A Mathematical Introduction to Robot Manipulation* (CRC, Boca Raton 1993)
- 38.20 D. Prattichizzo, A. Bicchi: Dynamic analysis of mobility and graspability of general manipulation systems, *IEEE Trans. Robotics Autom.* **14**(2), 241–258 (1998)
- 38.21 A. Bicchi: On the problem of decomposing grasp and manipulation forces in multiple whole-limb manipulation, *Int. J. Robotics Auton. Syst.* **13**, 127–147 (1994)
- 38.22 A.M. Dollar, R.D. Howe: Joint coupling and actuation design of underactuated hands for unstructured environments, *Int. J. Robotics Res.* **30**, 1157–1169 (2011)
- 38.23 L. Birglen, T. Laliberté, C. Gosselin: *Underactuated robotic hands*, Springer Tracts in Advanced Robotics (Springer, Berlin, Heidelberg 2008)
- 38.24 M.G. Catalano, G. Grioli, A. Serio, E. Farnioli, C. Piazza, A. Bicchi: Adaptive synergies for a humanoid robot hand, *Proc. IEEE–RAS Int. Conf. Humanoid Robots* (2012) pp. 7–14
- 38.25 M. Gabiccini, A. Bicchi, D. Prattichizzo, M. Malvezzi: On the role of hand synergies in the optimal choice of grasping forces, *Auton. Robots* **31**, 235–252 (2011)
- 38.26 M. Malvezzi, D. Prattichizzo: Evaluation of grasp stiffness in underactuated compliant hands, *Proc. IEEE Int. Conf. Robotics Autom.* (2013) pp. 2074–2079
- 38.27 S.F. Chen, I. Kao: Conservative congruence transformation for joint and cartesian stiffness matrices of robotic hands and fingers, *Int. J. Robotics Res.* **19**(9), 835–847 (2000)
- 38.28 M.R. Cutkosky, I. Kao: Computing and controlling the compliance of a robotic hand, *IEEE Trans. Robotics Autom.* **5**(2), 151–165 (1989)
- 38.29 A. Albu-Schaffer, O. Eiberger, M. Grebenstein, S. Haddadin, C. Ott, T. Wimbock, S. Wolf, G. Hirzinger: Soft robotics, *IEEE Robotics Autom. Mag.* **15**(3), 20–30 (2008)
- 38.30 A. Bicchi: Force distribution in multiple whole-limb manipulation, *Proc. IEEE Int. Conf. Robotics Autom.* (1993)
- 38.31 F. Reuleaux: *The Kinematics of Machinery* (Macmillan, New York 1876), Republished by Dover, New York, 1963
- 38.32 T. Omata, K. Nagata: Rigid body analysis of the indeterminate grasp force in power grasps, *IEEE Trans. Robotics Autom.* **16**(1), 46–54 (2000)
- 38.33 J.C. Trinkle: The Mechanics and Planning of Enveloping Grasps, Ph.D. Thesis (University of Pennsylvania, Department of Systems Engineering, 1987)
- 38.34 K. Lakshminarayana: *Mechanics of Form Closure*, Tech. Rep., Vol. 78–DET–32 (ASME, New York 1978)
- 38.35 E. Rimon, J. Burdick: Mobility of bodies in contact i: A 2nd order mobility index for multiple-finger grasps, *IEEE Trans. Robotics Autom.* **14**(5), 696–708 (1998)
- 38.36 B. Mishra, J.T. Schwartz, M. Sharir: On the existence and synthesis of multifinger positive grips, *Algoritmica* **2**(4), 541–558 (1987)
- 38.37 P. Somov: Über Schraubengeschwindigkeiten eines festen Körpers bei verschiedener Zahl von Stützflächen, *Z. Math. Phys.* **42**, 133–153 (1897)
- 38.38 P. Somov: Über Schraubengeschwindigkeiten eines festen Körpers bei verschiedener Zahl von Stützflächen, *Z. Math. Phys.* **42**, 161–182 (1897)
- 38.39 A.J. Goldman, A.W. Tucker: Polyhedral convex cones. In: *Linear Inequalities and Related Systems*, ed. by H.W. Kuhn, A.W. Tucker (Princeton Univ., York 1956) pp. 19–40
- 38.40 X. Markenscoff, L. Ni, C.H. Papadimitriou: The geometry of grasping, *Int. J. Robotics Res.* **9**(1), 61–74 (1990)
- 38.41 D.G. Luenberger: *Linear and Nonlinear Programming*, 2nd edn. (Addison–Wesley, Reading 1984)
- 38.42 G. Muscio, J.C. Trinkle: *Grasp Closure Analysis of Bilaterally Constrained Objects*, Tech. Rep. Ser., Vol. 13–01 (Department of Computer Science, Rensselaer Polytechnic Institute, Troy 2013)
- 38.43 Rensselaer Computer Science: <http://www.cs.rpi.edu/twiki/bin/view/RoboticsWeb/LabSoftware>
- 38.44 C. Ferrari, J. Canny: Planning optimal grasps, *Proc. IEEE Int. Conf. Robotics Autom.* (1986) pp. 2290–2295
- 38.45 V.D. Nguyen: *The Synthesis of Force Closure Grasps in the Plane*, M.S. Thesis Ser. (MIT Department of Mechanical Engineering, Cambridge 1985), AI–TR861
- 38.46 R.D. Howe, M.R. Cutkosky: Practical force–motion models for sliding manipulation, *Int. J. Robotics Res.* **15**(6), 557–572 (1996)
- 38.47 L. Han, J.C. Trinkle, Z. Li: Grasp analysis as linear matrix inequality problems, *IEEE Trans. Robotics Autom.* **16**(6), 663–674 (2000)
- 38.48 J.C. Trinkle: On the stability and instantaneous velocity of grasped frictionless objects, *IEEE Trans. Robotics Autom.* **8**(5), 560–572 (1992)
- 38.49 K.H. Hunt, A.E. Samuel, P.R. McAree: Special configurations of multi-finger multi-freedom grippers – A kinematic study, *Int. J. Robotics Res.* **10**(2), 123–134 (1991)
- 38.50 D.J. Montana: The kinematics of multi-fingered manipulation, *IEEE Trans. Robotics Autom.* **11**(4), 491–503 (1995)
- 38.51 Y. Nakamura, K. Nagai, T. Yoshikawa: Dynamics and stability in coordination of multiple robotic mechanisms, *Int. J. Robotics Res.* **8**, 44–61 (1989)
- 38.52 J.S. Pang, J.C. Trinkle: Stability characterizations of rigid body contact problems with coulomb friction, *Z. Angew. Math. Mech.* **80**(10), 643–663 (2000)

- 38.53 M.R. Cutkosky: *Robotic Grasping and Fine Manipulation* (Kluwer, Norwell 1985)
- 38.54 W.S. Howard, V. Kumar: On the stability of grasped objects, *IEEE Trans. Robotics Autom.* **12**(6), 904–917 (1996)
- 38.55 A.B.A. Cole, J.E. Hauser, S.S. Sastry: Kinematics and control of multifingered hands with rolling contacts, *IEEE Trans. Autom. Control* **34**, 398–404 (1989)
- 38.56 R.I. Leine, C. Glocker: A set-valued force law for spatial Coulomb–Contensou friction, *Eur. J. Mech. A* **22**(2), 193–216 (2003)
- 38.57 M. Buss, H. Hashimoto, J. Moore: Dexterous hand grasping force optimization, *IEEE Trans. Robotics Autom.* **12**(3), 406–418 (1996)
- 38.58 V. Nguyen: Constructing force-closure grasps, *Int. J. Robotics Res.* **7**(3), 3–16 (1988)
- 38.59 E. Rimon, J.W. Burdick: Mobility of bodies in contact II: How forces are generated by curvature effects, *Proc. IEEE Int. Conf. Robotics Autom.* (1998) pp. 2336–2341
- 38.60 R.B. McGhee, D.E. Orin: A mathematical programming approach to control of positions and torques in legged locomotion systems, *Proc. ROMANCY* (1976)
- 38.61 K. Waldron: Force and motion management in legged locomotion, *IEEE J. Robotics Autom.* **2**(4), 214–220 (1986)
- 38.62 T. Yoshikawa, K. Nagai: Manipulating and grasping forces in manipulation by multi-fingered grippers, *Proc. IEEE Int. Conf. Robotics Autom.* (1987) pp. 1998–2007
- 38.63 V. Kumar, K. Waldron: Force distribution in closed kinematic chains, *IEEE J. Robotics Autom.* **4**(6), 657–664 (1988)
- 38.64 M. Buss, L. Faybusovich, J. Moore: Dikin-type algorithms for dexterous grasping force optimization, *Int. J. Robotics Res.* **17**(8), 831–839 (1998)
- 38.65 D. Prattichizzo, J.K. Salisbury, A. Bicchi: Contact and grasp robustness measures: Analysis and experiments. In: *Experimental Robotics-IV, Lecture Notes in Control and Information Sciences*, Vol. 223, ed. by O. Khatib, K. Salisbury (Springer, Berlin, Heidelberg 1997) pp. 83–90
- 38.66 A.M. Dollar, R.D. Howe: The highly adaptive sdm hand: Design and performance evaluation, *Int. J. Robotics Res.* **29**(5), 585–597 (2010)
- 38.67 M.G. Catalano, G. Grioli, E. Farnioli, A. Serio, C. Piazza, A. Bicchi: Adaptive synergies for the design and control of the Pisa/IIT SoftHand, *Int. J. Robotics Res.* **33**(5), 768–782 (2014)
- 38.68 M.T. Ciocarlie, P.K. Allen: Hand posture subspaces for dexterous robotic grasping, *Int. J. Robotics Res.* **28**(7), 851–867 (2009)
- 38.69 T. Wimbock, B. Jahn, G. Hirzinger: Synergy level impedance control for multifingered hands, *IEEE/RSJ Int Conf Intell. Robots Syst. (IROS)* (2011) pp. 973–979
- 38.70 D. Prattichizzo, M. Malvezzi, M. Gabiccini, A. Bicchi: On the manipulability ellipsoids of underactuated robotic hands with compliance, *Robotics Auton. Syst.* **60**(3), 337–346 (2012)
- 38.71 D. Prattichizzo, M. Malvezzi, M. Gabiccini, A. Bicchi: On motion and force controllability of precision grasps with hands actuated by soft synergies, *IEEE Trans. Robotics* **29**(6), 1440–1456 (2013)
- 38.72 M.R. Dogar, S.S. Srinivasa: A framework for push-grasping in clutter, *Robotics Sci. Syst.* (2011)
- 38.73 M. Posa, R. Tedrake: Direct trajectory optimization of rigid body dynamical systems through contact, *Proc. Workshop Algorithm. Found. Robotics* (2012)
- 38.74 L. Zhang, J.C. Trinkle: The application of particle filtering to grasp acquisition with visual occlusion and tactile sensing, *Proc. IEEE Int. Conf Robotics Autom.* (2012)
- 38.75 P. Hebert, N. Hudson, J. Ma, J. Burdick: Fusion of stereo vision, force-torque, and joint sensors for estimation of in-hand object location, *Proc. IEEE Int. Conf. Robotics Autom.* (2011) pp. 5935–5941
- 38.76 S. Haidacher, G. Hirzinger: Estimating finger contact location and object pose from contact measurements in 3rd grasping, *Proc. IEEE Int. Conf. Robotics Autom.* (2003) pp. 1805–1810
- 38.77 T. Schlegl, M. Buss, T. Omata, G. Schmidt: Fast dextrous re-grasping with optimal contact forces and contact sensor-based impedance control, *Proc. IEEE Int. Conf. Robotics Autom.* (2001) pp. 103–108
- 38.78 G. Muscio, F. Pierri, J.C. Trinkle: A hand/arm controller that simultaneously regulates internal grasp forces and the impedance of contacts with the environment, *IEEE Conf. Robotics Autom.* (2014)
- 38.79 M.A. Roa, R. Suarez: Computation of independent contact regions for grasping 3-D objects, *IEEE Trans. Robotics* **25**(4), 839–850 (2009)
- 38.80 M.A. Roa, R. Suarez: Influence of contact types and uncertainties in the computation of independent contact regions, *Proc. IEEE Int. Conf. Robotics Autom.* (2011) pp. 3317–3323
- 38.81 A. Rodriguez, M.T. Mason, S. Ferry: From caging to grasping, *Int. J. Robotics Res.* **31**(7), 886–900 (2012)
- 38.82 C. Davidson, A. Blake: Error-tolerant visual planning of planar grasp, *6th Int. Conf. Comput. Vis.* (1998) pp. 911–916